

Emergence of radial orientation selectivity: Effect of cell density changes and eccentricity in a layered network

Catherine E. Davey^a, David B. Grayden^a, and Anthony N. Burkitt^a

^a*Department of Biomedical Engineering, The University of Melbourne, VIC 3010, Australia*

December 4, 2020

Keywords: neural network, rate-based neural plasticity, orientation selectivity, spatial opponent cells

Abstract

An account of how simple cells can emerge in the absence of structured environmental input via a self-organised learning process has been provided by Linsker (1986); this work empirically showed the emergence of spatial-opponent cells as a result of structure in the initial synaptic connectivity distribution when the visual system is driven entirely by input noise. In this paper, the complete set of eigenfunctions and eigenvalues for a three-layer network is analytically derived for the first time. As a first step, a simplified learning equation is considered for which the homeostatic parameters are set to zero. This is then extended to an analysis of the eigenfunctions of the full learning equation, including non-zero homeostatic parameters, using a perturbation analysis. These results extend the previous analysis of the Linsker (1986) network to allow for radially dependent cell density, as found in the retina. The results establish that radially biased orientation selectivity emerges in the third layer when cell density in the first layer changes with eccentricity; i.e., distance to the centre of the lamina. This provides a potential mechanism for the emergence of radial orientation in the primary visual cortex before eye opening and the onset of structured visual input after birth.

1 Introduction

Synaptic plasticity underpins our understanding of learning in neural systems as it is the mechanism that describes how synaptic weights change in response to sensory inputs. Plasticity has traditionally been modelled as rate based, in which synaptic weights change in response to short-time averaged pre- and postsynaptic neuron spiking rates. Over the past two decades, the importance of pre- and postsynaptic neuron spike timing has been recognized, particularly for contexts in which high-resolution temporal information is involved at microsecond resolution (Kempster et al., 1999a; Gerstner et al., 1996), prompting the emergence of spike-timing dependent plasticity (STDP) (Gerstner et al., 1996; Markram et al., 1997). Spike-based plasticity updates synaptic strength in response to the relative timing of pre- and postsynaptic spikes, amplifying synaptic strength if the presynaptic neuron contributes to the postsynaptic neuron's spike, and depressing a synapse if the presynaptic neuron fires after the postsynaptic neuron and thus did not contribute to its spike.

Plasticity mechanisms have played a fundamental role in explaining the emergence of simple cells in the early layers of cortical processing, such as the primary visual cortex (V1). Plasticity has successfully explained the emergence of simple cells such as orientation selective cells (Bienenstock et al., 1982; Wimbauer et al., 1998; Yamakazi, 2002), direction selective cells (Wimbauer et al., 1997a,b; Senn and Buchs, 2003), ocular dominance (Miller, 1990), and feature maps in which sensitivity to a particular feature changes as the layer is traversed (Goodhill, 2007).

Much of the research on learning in cortical networks has been empirical and computational because of the analytical complexity of learning in response to parameters that describe the number of layers, connectivity structure, and neuron type. A

notable exception is the analysis of the network proposed by Linsker (1986a) in which the emergence of a spatial opponent cell in the third layer of a three-layer network of Poisson neurons with Gaussian connectivity kernels was described. Learning in this network is a linear function of correlation in presynaptic neural activity, with two learning constants that control the homeostatic equilibrium. The linearity of the learning system enables an eigenfunction analysis to be used to identify the independent contributors to a postsynaptic neuron's synaptic weight structure. Eigenvalues provide a way to distinguish the eigenfunctions that are the most significant contributors, and hence determine the receptive field of the postsynaptic neuron.

Although Linsker (1986a) focused on empirical results, there has been significant work aimed at extending the analytical framework for the network that he proposed. MacKay and Miller (1990) proposed the first three radial eigenfunctions based on the work by Tang (1990), but without providing a derivation. The proposed eigenfunctions were for a simplified learning system in which homeostatic constants were assumed zero so that all plasticity was driven by correlation between presynaptic inputs and there was no non-competitive plasticity. They provided an empirical examination of the impact of non-zero homeostatic constants, showing that the eigenfunction of the leading eigenvalue can change in response to a change in the homeostatic equilibrium.

Miller (1990) employed Linsker's (1986a) network in a model of learning in the primary visual cortex, with overlapping left and right eye inputs processed by the lateral geniculate nucleus (LGN). The network structure prompted correlation and anti-correlation in two afferents originating from either the same eye or the opposite eye, leading to the emergence of an ocular dominance feature map. Miller (1990) provided a description of an analytical derivation for the eigenfunctions of ocular dominance feature maps across the cortex.

Wimbauer et al. (1998) extended Linsker's (1986a) network by incorporating lateral inhibitory connections in the third layer, showing the emergence of orientation selective cells in the third layer. They provided a derivation of Cartesian eigenfunctions for learning with homeostatic constants set to zero and empirically extended the solution to the general learning equation with non-zero homeostatic constants. They simulated the development of an orientation selective feature map distributed across the primary visual cortex using a model slightly more complex than that for which they derived the eigenfunctions.

Analytical solutions to Linsker's (1986a) learning system have played a central role in explaining the emergence of spatial opponent and orientation selective cells in the network. However, thus far, no general analytical solution has been provided, with analytical results to date being for the simplified system in which the homeostatic constants are set to zero. We provide here a solution for the eigenfunctions of Linsker's (1986a) network in polar coordinates. As the system is radially symmetric, polar coordinates provide a natural coordinate system that enables a straightforward extension of polar eigenfunctions to the general learning system with non-zero homeostatic constants. One of the benefits of a full analytical solution for the network is insight into why the receptive field changes in response to changes in the homeostatic equilibrium and the framework to determine exactly when this change occurs.

Thus far, the original network proposed by Linsker (1986a) and used in the subsequent analytical analyses of Miller (1990) and Wimbauer et al. (1998) made an assumption that cells within each layer were evenly distributed and that receptive fields of all cells in a layer were statistically identical; i.e., drawn from the same synaptic connectivity distribution. To date, there has been no exploration of the impact of relaxing this assumption. However, it is known that some biological cell layers show an uneven density of cells across the lamina and contain receptive fields with different statistical properties. For example, the retina is well known to have cell density changes as a function of eccentricity (Sjöstrand et al., 1999; Watson, 2014) and receptive field sizes of neurons in the primary visual cortex increase with stimulus eccentricity (Wurbs et al., 2013; Smith et al., 2001). Furthermore, it is well established that orientation selectivity in the primary visual cortex is biased towards radial orientation in that an orientation selective neuron in the primary visual cortex is more likely to be oriented towards the centre of the retina (Rodionova et al., 2004). In this study, we explore the impact of radially dependent synaptic connection distributions on emerging receptive field properties in the third layer of Linsker's (1986a) network and show how introducing radially dependent synaptic connectivity distributions in the first layer results in the emergence of radial orientation selectivity in the third layer of the network.

This paper is organised as follows. Section 2.1 introduces the network and neuron models used, based on Linsker's (1986a) network. Radial eigenfunctions and eigenvalues are analytically derived for the simplified learning equation, for which the homeostatic parameters are set to zero, and then extended via perturbation analysis to the full system in Section 3. Eigenfunctions and eigenvalues are also derived in Cartesian coordinates in Section 3 and compared to the radial eigenfunctions. Finally, we show in Section 4 that the introduction of radially dependent synaptic connectivity distributions in the first layer generates radial orientation selectivity in the third layer of the network.

2 Methods

2.1 Network specification

Following Linsker (1986a), we consider a three-layer, feed-forward topographical network. The network is driven by spontaneous neural activity in the first layer, layer A , which inputs to layer B , which in turn inputs to layer C , as shown schematically in Fig. 1. Layers comprise populations of homogeneous neurons, equispaced in a square grid across the layer. The distance between the parallel layers is assumed to dominate sufficiently such that propagation delay experienced by action potentials from the presynaptic layer can be assumed approximately equal. Neurons m and n of layer A have synaptic inputs to neurons i and j of layer B , respectively, which both input to neuron p of layer C .

Each postsynaptic neuron has a Gaussian synaptic connection distribution, centred on its two-dimensional position in the lamina, which ensures that radially proximate neurons are more likely to connect to it than a neuron more distal in the presynaptic lamina. The connectivity distributions are parameterised by a standard deviation (radius) that is homogeneous across a layer, denoted σ^{AB} and σ^{BC} , for synaptic connections between layers A and B and layers B and C , respectively. Consequently, the probability of neuron m in layer A connecting to neuron i in layer B is given by

$$p_N \left((x_{mi}, y_{mi}); \frac{1}{2}(\sigma^{AB})^2 \right) = \frac{1}{\pi(\sigma^{AB})^2} \exp \left(-\frac{x_{mi}^2 + y_{mi}^2}{(\sigma^{AB})^2} \right), \quad (1)$$

where (x_{mi}, y_{mi}) is the two-dimensional radial distance between m and i . Note that this definition differs from the standard definition by a factor of $\sqrt{2}$ in accordance with the definition used by Linsker (1986a), and is specifically chosen for later convenience.

For postsynaptic neurons in layer C , it is useful to write the connection probability in polar coordinates by assuming, without loss of generality, that the postsynaptic neuron is at position $(0,0)$. The probability of presynaptic neuron j in layer B connecting to postsynaptic neuron p in layer C in polar coordinates is then

$$p_N \left((r_{jp}, \theta_{jp}); \frac{1}{(\sigma^{BC})^2} \right) = \frac{1}{\pi(\sigma^{BC})^2} \exp \left(-\frac{r_{jp}^2}{(\sigma^{BC})^2} \right), \quad (2)$$

where r_{jp} is the radial distance from the centre of the lamina to neuron i in layer C , and θ_{jp} is the angle to i within the two-dimensional lamina.

Linsker (1986a) showed that the Gaussian connectivity distributions introduce spatial correlations in the inputs to layer B neurons despite spontaneous neural activity in layer A being uncorrelated. Layer B neurons that are spatially more proximate will have a greater number of shared connections, and therefore more correlated input, when compared to layer B neurons that are positioned further apart in the lamina. The expected number of shared presynaptic inputs between two postsynaptic neurons in layer B is shown to be (see Appendix A for full derivation)

$$\mathbb{E} \left[N^{BB}(d) \right] = \frac{(N^{AB})^2}{2\pi(\sigma^{AB})^2} \exp \left(-\frac{(d_{ij}^B)^2}{2(\sigma^{AB})^2} \right), \quad (3)$$

where N^{AB} denotes the expected number of synaptic connections from layer A to each neuron in layer B , and d_{ij}^B represents the distance between neurons i and j such that $d_{ij}^B = \sqrt{x_{mi}^2 + y_{mi}^2}$.

2.2 Neuron model

The network is driven by spontaneous Poisson activity of the layer A neurons. This implies that there are no spike-based temporal correlations between input and output neurons other than what is captured in the rate-based signals and that the rates change slowly when compared to the period over which they are averaged (Kempster et al., 1999b). Activity of a layer A neuron is modelled as $f_m^A(t) \sim \text{Poisson}(\lambda^A)$, where $f_m^A(t)$ is the spiking rate of layer A neuron m at time t .

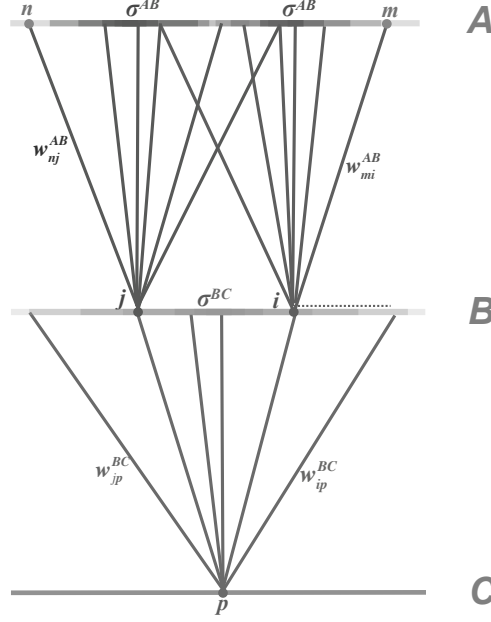


Figure 1: Schematic diagram of the three layered feed-forward network. Layer A neurons, m and n , feed into layer B neurons, i and j , respectively, which in turn feed to a layer C neuron, p (green). Synaptic connections between neurons are shown as solid, coloured lines connecting from a presynaptic neuron to a postsynaptic neuron of the same colour. The synaptic strength, for example between neurons m and i , is denoted w_{mi}^{AB} . Synaptic connection distributions are homogeneous within a layer and modelled as being Gaussian, parameterised by distance-dependent standard deviation (radius) denoted σ^{AB} between layers A and B and σ^{BC} between layers B and C. The probability of a postsynaptic neuron having a presynaptic connection from a particular position in the layer is depicted by the intensity of the colour of the presynaptic layer. Not shown in the diagram is the expected number of presynaptic connections input to a neuron, denoted by N^{AB} and N^{BC} for postsynaptic neurons in layers B and C, respectively. The radial distance between two neurons within a lamina, for example between neuron m from layer A and i from layer B, is denoted d_{mi}^B .

As in Linsker (1986a), we use a Poisson neuron model so that the network is linear when operating within the weight bounds, discussed below. The update equations for neural activity in layers B and C are

$$f_i^B(t) = R_a^B + \sum_m w_{mi}^{AB}(t) f_m^A(t), \quad (4a)$$

$$f_p^C(t) = R_a^C + \sum_i w_{ip}^{BC}(t) f_i^B(t), \quad (4b)$$

where R_a^B , R_a^C denote spontaneous firing rates, and $w_{mi}^{AB}(t)$, $w_{ip}^{BC}(t)$ depict synaptic strengths between neurons m and i in layers A and B, respectively, and neurons i and p in layers B and C, respectively. Note that an implicit assumption in this Poisson model of neural activity is that propagation delay is negligible or, equivalently, is dominated by inter-layer distances between neurons and, therefore, can be considered homogeneous across all inputs to a postsynaptic neuron.

2.3 Learning dynamics

The adiabatic approximation in neural learning is that incremental weight changes occur slowly with respect to neural dynamics, which occur on a millisecond timescale. Furthermore, neurons within the same population are assumed to have the same statistical properties of neural activity and synaptic connectivity. Consequently, the system is ergodic and the spike rate can be determined from the ensemble average or from a temporal mean over the timescale of learning. Under these assumptions, the learning equation can be expressed as a differential equation (Linsker, 1986a). The general learning equations for synaptic

weights between neurons in layers A and B and synapses connecting layers B and C is given by (Linsker, 1986a)

$$\eta \dot{w}_{mi}^{AB} = k_1^{AB} + \frac{1}{N^{AB}} \sum_n w_{ni}^{AB} (Q_{mn}^A + k_2^{AB}), \quad w_{\min} \leq w_{mi}^{AB} \leq w_{\max}, \quad (5a)$$

$$\eta \dot{w}_{ip}^{AB} = k_1^{BC} + \frac{1}{N^{BC}} \sum_j w_{jp}^{BC} (Q_{ij}^B + k_2^{BC}), \quad w_{\min} \leq w_{mi}^{AB} \leq w_{\max}, \quad (5b)$$

where $\eta \ll 1$ is the learning rate that ensures that learning is slow on a millisecond timescale, w_{\min} and w_{\max} are the lower and upper bounds on the weights, respectively, and the parameters k_1^{AB} , k_2^{AB} , k_1^{BC} , k_2^{BC} are layer specific constants controlling homeostasis (i.e., independent of the correlation structure of the inputs). The definition for normalised covariance has the same structure for each layer; for example, the normalised covariance Q_{mn}^A between layer A neurons m and n is defined by

$$Q_{mn}^A = \frac{\langle f_m^A - \bar{f}^A \rangle \langle f_n^A - \bar{f}^A \rangle}{f_0^2}, \quad (6)$$

where $\langle \rangle$ depicts the ensemble average, \bar{f}^A denotes the temporal average of layer A neural activity, and f_0^2 is a scaling factor to normalise the covariance matrix Q .

For a Gaussian synaptic density distribution, the covariance between layer B neurons is a function of the radial distance separating the neurons, as described in Appendix B,

$$\text{cov}(f_m^B, f_n^B) = \frac{(N^{BC} \sigma^A)^2}{2\pi(\sigma^{AB})^2} \exp\left(-\frac{d_{mn}^B}{2(\sigma^{AB})^2}\right). \quad (7)$$

Note that vector distances are given with respect to the layer C cell, so we define the two-dimensional radial distance of presynaptic neuron, m , from postsynaptic neuron, i , by vector, $\mathbf{x}_{mi} = [x_{mi}, y_{mi}]^T$, and $d_{ij}^B = \|\mathbf{x}_{mi} - \mathbf{x}_{ni}\|$. Only radial distances are considered, so that distances between layers are assumed to have negligible impact on learning dynamics since the inter-layer transmission delay is uniform.

Normalising this result and incorporating it into Eq. (5) gives the learning equation

$$\eta \dot{w}_{mi} = k_1 + \frac{1}{N} \sum_n w_{ni} \left(\exp\left(-\frac{|\mathbf{x}_{mi} - \mathbf{x}_{ni}|^2}{2(\sigma^{AB})^2}\right) + k_2 \right), \quad (8)$$

where it is assumed that the covariance is normalised and we have removed the layer superscripts for readability.

It is assumed that a deeper layer is not learned until after its presynaptic layer has converged to a stable weight structure, and hence layers are learned sequentially. This accords with the approach employed by (Linsker, 1986a) and does not impact the final weight structure across the network. Consequently, synapses connecting layers A and B evolve to a stable structure before learning begins for synapses connecting layers B and C .

Linsker (1986a) demonstrated that individual synapses are unstable and, for excitatory synapses, all or all-but-one necessarily reach the upper bound, w_{\max} . However, under an assumption of weak covariance of the inputs (MacKay and Miller, 1990), the mean weight of synapses input to a postsynaptic neuron is not necessarily unstable but rather controlled by homeostatic mechanisms. For excitatory connections, the mean weight of a postsynaptic neuron's synapses will converge to

$$\bar{w} = -\frac{k_1}{k_2}, \quad \text{if } k_2 < 0, \quad \text{and } 0 < \frac{k_1}{k_2} < 1, \quad (9)$$

where the conditions on k_1 and k_2 are required to ensure that the mean synaptic weight does not diverge to the bounds. For all synapses to grow until they reach the upper bound, it is required that $k_1 + k_2 > 0$. In this case, the system is unstable so that the mean synaptic weight grows until all individual synapses, or all-but-one, have reached the upper bound (Linsker, 1986a).

Linsker (1986a) selected homeostatic constants for synapses connecting layers A and B such that the mean weight was unstable and, consequently, all synapses diverged to the upper bound. For connections between layers B and C , the homeostatic constants are chosen such that the mean weight is stable, requiring some individual synapses to diverge to the lower bound and others to the upper bound.

With synaptic connections between layers A and B assumed to all reach the upper bound, the focus is on determining the learned synaptic structure for postsynaptic neurons in layer C . Given that the learning equation in Eq. (5b) is linear within the

weight bounds, the system lends itself to an eigenfunction analysis. That is, we wish to identify the independent eigenfunctions that contribute to the evolution of synaptic weights. Given that the system is driven by unstructured noise, it will self-organise such that the eigenfunction with the leading eigenvalue will ultimately dominate the synaptic weight structure.

In order to conduct an eigenfunction analysis, we approximate the discrete grid of neurons by its continuous limit. The probability of a synaptic connection existing between neuron m at position (x_{mi}, y_{mi}) in the presynaptic layer and postsynaptic neuron i , detailed in Eq. (1), becomes a synaptic density describing the expected proportion of the total number of presynaptic inputs originating from (x_{mi}, y_{mi}) . The synaptic strength is then considered to be the average weight of synapses at this location. In the continuous limit, the learning equation in Eq. (8) becomes

$$\eta w(\mathbf{x}) = k_1 + \int_{-\infty}^{\infty} A \left(\exp\left(-\frac{|\mathbf{x} - \mathbf{x}'|^2}{2(\sigma^{AB})^2}\right) + k_2 \right) \exp\left(-\frac{|\mathbf{x}'|^2 + |\mathbf{x}|^2}{(\sigma^{BC})^2}\right) w(\mathbf{x}') d^2 \mathbf{x}', \quad (10)$$

where neuron i in layer B is denoted by its continuous position vector $\mathbf{x} = (x_{ip}, y_{ip})$ and neuron j in layer B is represented by its continuous vector, $\mathbf{x}' = (x_{jp}, y_{jp})$, where subscripts have been omitted for readability. The Cartesian coordinates have been centred on the layer C neuron. Note that A contains coefficients to normalise covariance and connection probabilities, such that $A = (\pi(\sigma^{BC})^2)^{-2}$.

To characterise the system in terms of its eigenfunctions, we need to solve the eigenvalue problem for the system,

$$\lambda \eta w(\mathbf{x}) = \int_{-\infty}^{\infty} A \left(\exp\left(-\frac{|\mathbf{x} - \mathbf{x}'|^2}{2(\sigma^{AB})^2}\right) + k_2 \right) \exp\left(-\frac{|\mathbf{x}'|^2 + |\mathbf{x}|^2}{(\sigma^{BC})^2}\right) w(\mathbf{x}') d^2 \mathbf{x}'. \quad (11)$$

3 Radial eigenfunctions of the learning equation

Given the circular symmetry of the spatial opponent neurons that emerge from Linsker's (1986a) network, we derive the radial eigenfunctions and eigenvalues of a layer C neuron's receptive field. By identifying the eigenfunction with the largest eigenvalue, we can analytically determine the expected receptive field of the neuron, since this eigenfunction is expected to grow most rapidly and dominate development of the receptive field.

3.1 Radial eigenfunctions of the simplified learning equation

To proceed we initially set k_2 to zero and later consider the more general case in which k_2 is non-zero. Converting to polar coordinates, such that r and θ give the magnitude and phase of \mathbf{x} , and transforming r to be unit-less by scaling it by $\frac{1}{\sigma^{AB}}$, the eigenvalue problem in Eq. (11) becomes

$$\begin{aligned} \lambda \eta w(r, \theta) = & A(\sigma^{AB})^2 \exp\left(-\frac{r^2}{2} \left(\frac{2(\sigma^{AB})^2 + (\sigma^{BC})^2}{(\sigma^{BC})^2}\right)\right) \int_0^{\infty} d\tilde{r} \tilde{r} \exp\left(-\frac{\tilde{r}^2}{2} \left(\frac{2(\sigma^{AB})^2 + (\sigma^{BC})^2}{(\sigma^{BC})^2}\right)\right) \\ & \int_0^{2\pi} d\tilde{\theta} \exp\left(-\frac{-2r\tilde{r}\cos(\theta - \tilde{\theta})}{2}\right) w(\tilde{r}, \tilde{\theta}). \end{aligned} \quad (12)$$

The eigenfunctions and eigenvalues for the simplified learning equation are derived in Appendix C.1. Introducing a radial decay parameter that controls the rate of decay from the centre of the receptive field,

$$C = \frac{(\sigma^{BC})^2}{2\sigma^{AB}\sqrt{(\sigma^{AB})^2 + (\sigma^{BC})^2}}, \quad (13)$$

the eigenfunctions and associated eigenvalues can be expressed in polar coordinates as

$$\lambda_{l,n} = 2\pi A \left(\frac{C(\sigma^{BC})^2}{C((\sigma^{AB})^2 + (\sigma^{BC})^2) + (\sigma^{BC})^2} \right)^{l+n+1} \quad (14a)$$

$$\mathbf{v}_{l,n}(r, \theta) = N_{l,n} r^{l-n} \exp\left(-\frac{r^2}{2C}\right) L_n^{l-n}\left(\frac{r^2}{C}\right) \exp(i(l-n)\theta), \quad (14b)$$

where $N_{l,n}$ is a normalisation factor and L_n^{l-n} is an associated Laguerre polynomial. Since $\int_0^\infty x^p e^{-x} L_q^p(x)^2 dx = (p+q)!/q!$, the normalisation factor can be derived as

$$N_{l,n} = \begin{cases} \sqrt{\frac{2}{\pi C(\sigma^{AB})^2}}, & l = n \\ \sqrt{\frac{n!}{\pi l! C^{l-n+1} (\sigma^{AB})^2}}, & \text{otherwise,} \end{cases} \quad (15)$$

where the factor of 2 difference occurs for the case $l = n$ because the integral for the angular component is over $\cos(0\theta)$, a constant.

Eigenfunctions up to order 4 are shown in Fig. 2 in order of decreasing eigenvalue, λ . The eigenfunctions are ordered by $l+n$, where n controls the shape of the Laguerre polynomial and $l-n$ controls the angular frequency. The eigenfunction with the largest eigenvalue has order $l+n=0$ and is radially symmetric with all positive synaptic weights. Consequently, for the simplified learning equation described in Eq. (12) and after learning for a sufficiently long period, the synaptic weight structure of a layer C postsynaptic neuron will be all excitatory connections with weights at the upper bound.

For completeness, we derive the eigenfunctions and eigenvalues of Linsker's (1986a) network using Cartesian coordinates, the solution of which is a special case of that found in Wimbauer et al. (1997b). We show that a weighted sum of the Cartesian eigenfunctions produces the radial eigenfunctions, thus establishing equivalence. The derivations are given in Appendix D. For eigenvalues indexed by order u and v , for the x and y dimensions respectively, eigenfunction and eigenvalue pairs are given by

$$\lambda_{u,v} = 2\pi(\sigma^{AB})^2 q^{u+v+1} \quad (16a)$$

$$\mathbf{v}_{u,v}\left(\frac{x}{\sqrt{C}}, \frac{y}{\sqrt{C}}\right) = \frac{1}{\sqrt{2^u u!}} \frac{1}{\sqrt{2^v v!}} H_u\left(\frac{x}{\sqrt{C}}\right) H_v\left(\frac{y}{\sqrt{C}}\right) \exp\left(-\frac{x^2 + y^2}{2C}\right). \quad (16b)$$

Fig. 3 shows Cartesian eigenfunctions up to the fourth order, which is determined by $u+v$. The eigenfunctions are shown in order of decreasing eigenvalue, so that the eigenfunction with the largest eigenvalue is of order $u+v=0$. This eigenfunction is radially symmetric, with all positive weights. Consequently, the Cartesian eigenfunctions of the simplified learning equation described in Eq. (61) give the same result as the radial eigenfunctions, shown in Fig. 2. After sustained learning, the weight structure of a neuron in layer C will have all synapses at the upper bound.

3.2 Radial eigenfunctions of the full learning equation

While covariance between the activity of layer B input neurons primarily drives the structure of the layer C cell, the k_1^{BC} and k_2^{BC} terms control the homeostatic equilibrium. MacKay and Miller (1990) empirically showed that the choice of k_2^{BC} can change the structure of the dominant eigenfunction, and hence the resultant receptive field of a layer C cell. As Fig. 2 shows, for the simplified system, the leading eigenvalue has all synapses at the upper or the lower bound. For a negative value of k_2^{BC} , homeostasis can only be reached if some of the synapses are negative. To determine the impact of the learning constant, we find an analytical expression for the eigenfunctions of the full learning equation, Eq. (11), by conducting a perturbation analysis on the simplified learning equation, in Eq. (11).

The full derivation is detailed in Appendix C.2. The eigenfunctions of the first order perturbation are equal to those of the simplified equation, Eq. (14b). However, the eigenvalues are altered by the addition of the learning constants according to

$$\lambda_{l,n}^1 = \lambda_{l,n} + W_{l,n}, \quad (17)$$

where

$$W_{l,n} = \pi C^{l-n+1} k_2^{BC} N_{l,n}^2 \frac{\Gamma(l+n+1)(\alpha-1)^{2n}}{n!^2 \alpha^{l+n+1}} {}_2F_1\left(-n, n; l-n; \frac{\alpha(\alpha-2)}{(\alpha-1)^2}\right), \quad (18)$$

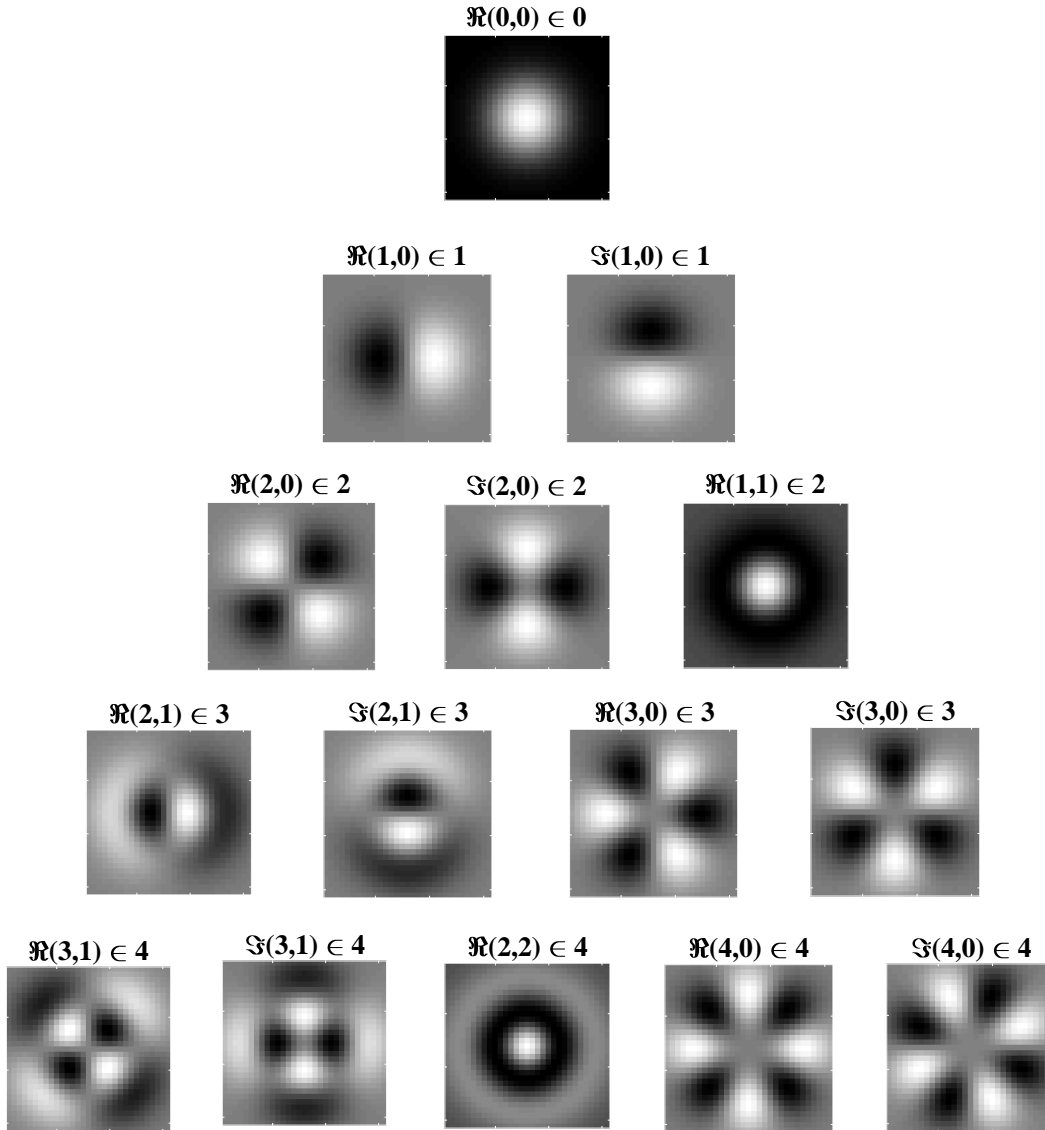


Figure 2: Eigenvalues and eigenfunctions of the simplified learning equation, Eq. (12), given in Eq. (14) for pairs of indices, $(l, n) \in \lambda_{l,n}$. Eigenvalues are ordered by $l+n$, with $l+n=0$ giving the largest eigenvalue and, hence, $(0,0)$ being the leading eigenfunction. Eigenfunctions in the same row have the same eigenvalue and are, therefore, degenerate. Eigenfunctions are given for both the real part of Eq. (14b) (i.e., the cosine angular component) and for the imaginary part, denoted by \Re and \Im , respectively. From the figure, it can be seen that, when $l=n$, the eigenfunction is radially symmetric, being fully determined by the radial component of the eigenfunction. White indicates positive regions of synaptic weights, while black indicates negative regions. The leading eigenfunction is all positive. As $l-n$ increases, the frequency of the angular component increases.

and ${}_2F_1(\cdot)$ is the hypergeometric function. As detailed in Appendix C.2, the only non-zero perturbations are where $l+n$ is even and $l=n$, which happens only once for each even order degenerate eigenfunction set.

Inspection of Eq. (18) reveals that, for positive k_2 , perturbation of the eigenvalues is positive and monotonically decreasing with $l+n$. Consequently, the order of the eigenvalues remains the same. For negative k_2 , the perturbation on the eigenvalues is negative and monotonically increasing with eigenfunction order, $l+n$. Since these perturbations are being added to the original eigenvalues, which are positive, the result can be a change in the dominant eigenfunction. This result supports the empirical findings by MacKay and Miller (1990) who showed the emergence of a spatial opponent cell in C , where $l+n=0$ for small values of k_2 , and bi-lobed neurons with $l+n=1$, for larger values of k_2 .

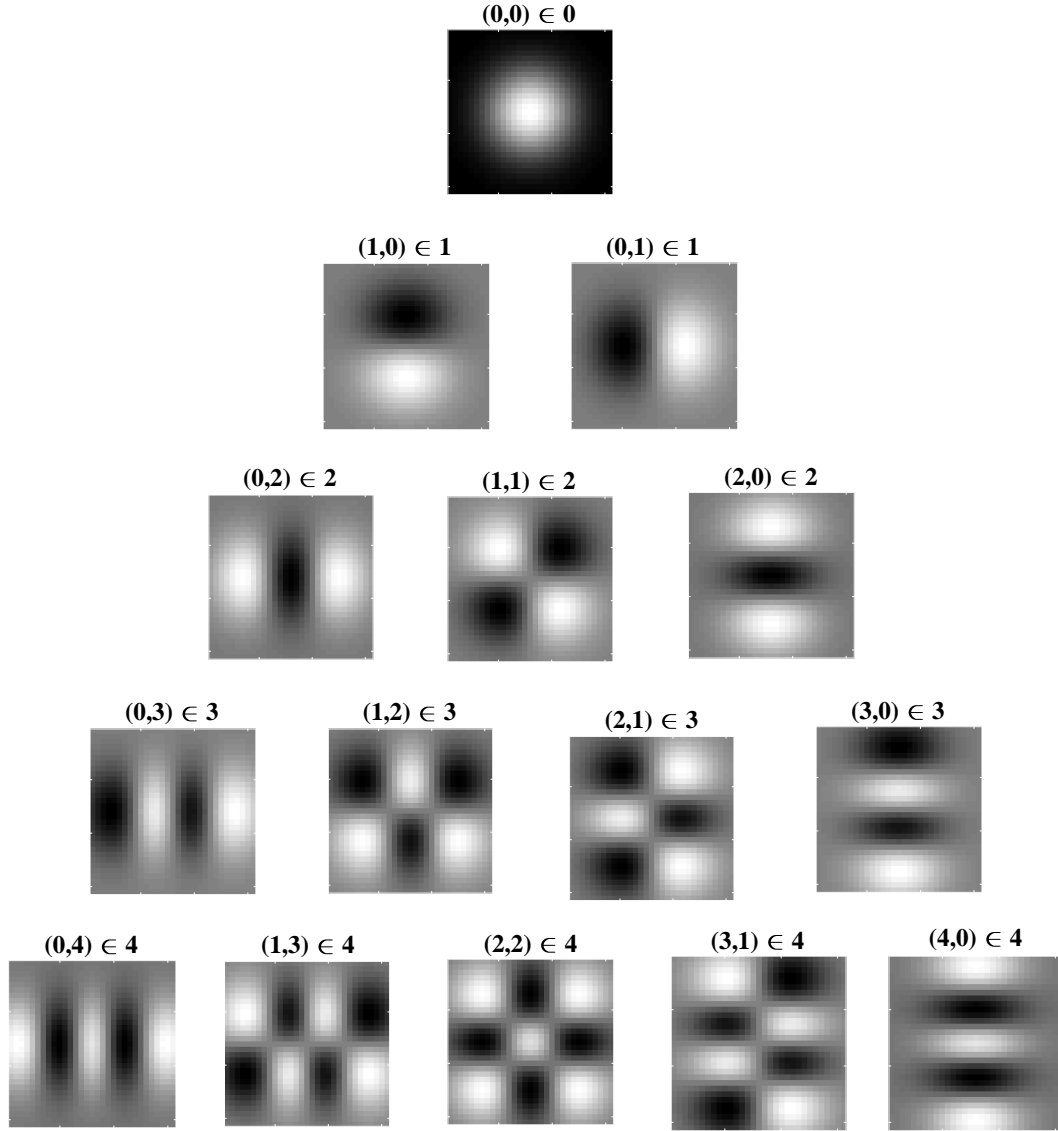


Figure 3: Cartesian eigenfunctions of the simplified learning equation, Eq. (61), defined for index pairs (u, v) . Eigenvalues are determined by $u + v$, where $(0, 0)$ has the largest eigenvalue and therefore $v_{0,0} \left(\frac{x}{\sqrt{C}}, \frac{y}{\sqrt{C}} \right)$ is the leading eigenfunction. Eigenfunctions in the same row have the same eigenvalue and are, therefore, degenerate. Eigenvalues decrease with descending rows. Regions of white indicate positive synaptic weights, while black indicates negative weights. The leading eigenfunction has all positive synapse weights.

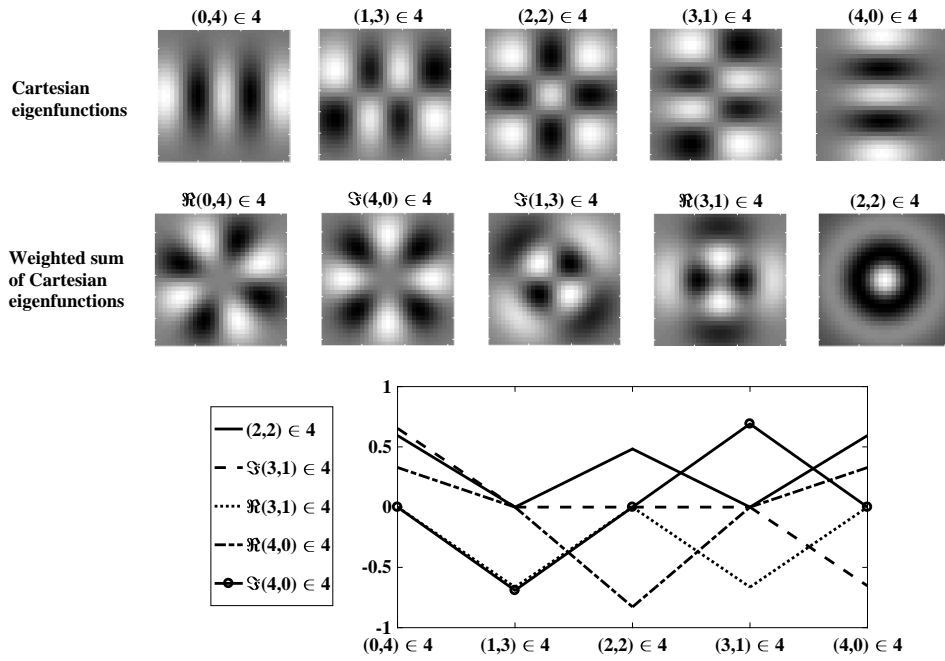


Figure 4: A weighted sum of degenerate Cartesian eigenfunctions of order $u+v=4$ are used to generate radial eigenfunctions of order $l+n=4$. Weights are determined using maximum likelihood regression. The top row shows degenerate Cartesian eigenfunctions of order 4. The middle row shows the weighted sum of the Cartesian eigenfunctions, reproducing the radial eigenfunctions in Fig. 2. The bottom row shows the regression weights.

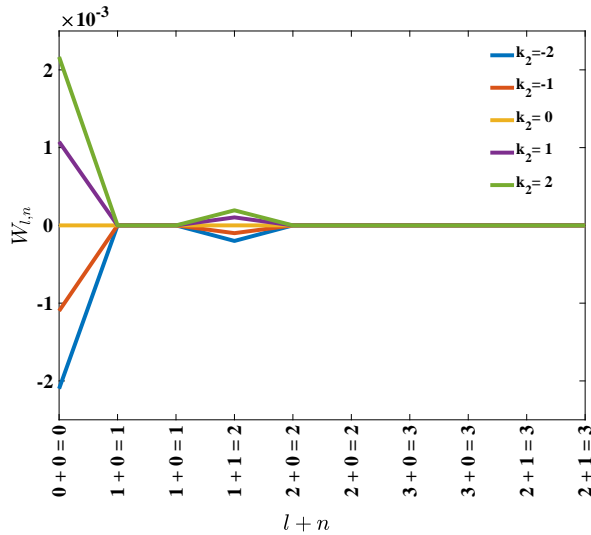


Figure 5: Effect of adding the perturbation term, k_2 , on eigenvalues $\lambda_{l,n}$, represented by $W_{l,n}$ in Eq. (17). For positive k_2 , the perturbation results in $W_{l,n}$ being positive, while for negative k_2 , the perturbation causes $W_{l,n}$ to be negative.

4 Emergence of radial orientation selectivity

The original network proposed by Linsker (1986a), and for which we have calculated the eigenfunctions, made an implicit assumption that neurons within each layer were evenly distributed and that receptive fields of all neurons in a layer were statistically identical, drawn from the same synaptic connectivity distribution. However, it is known that some biological neuron layers show an uneven density of cells across the lamina, and contain receptive fields with different statistical properties.

We consider the impact of changing neuron density as a function of distance to the layer centre. We assume that a consequence of this is that the radius of a neuron's synaptic connectivity distribution becomes dependent on the neuron's position in the layer. That is, where neurons are spread further apart there is an increase in connectivity radius to compensate. For simplicity assume that a postsynaptic neuron's arbor is within a sufficiently small area that the presynaptic neuron connection density is parameterised by a constant radius. If we denote the spatial centre of the neuron layer by c and consider this point to have location vector $[0, 0]$, then a postsynaptic cell, located at $[x_{ic}, y_{ic}]$, has connection density that is a function of the magnitude of its position,

$$d_{ic}^B = (x_i^2 + y_i^2)^{1/2}. \quad (19)$$

Let the radius of a cell be a linear function of its radial distance to the layer centre, such that

$$\sigma_i^{AB} = d_{ic}^B \sigma^{AB}. \quad (20)$$

In this scenario, the probability of presynaptic neuron, m , in layer A , generating a synaptic connection to postsynaptic neuron, i , in layer B , is given by

$$p_N \left((x_{mi}, y_{mi}); \frac{1}{2} (\sigma^{AB})^2 \right) = \frac{1}{\pi (d_{ic}^B)^2 (\sigma^{AB})^2} \exp \left(-\frac{x_{mi}^2 + y_{mi}^2}{(d_{ic}^B)^2 (\sigma^{AB})^2} \right). \quad (21)$$

In Appendix E, we calculate the expected number of shared inputs between two neurons in layer B . This is important to consider as shared inputs is the source of correlation between layer B neurons, which then triggers the emergence of spatial opponent neurons in Linsker's (1986a) network. In the case of the synaptic connection radius increasing linearly with distance from the centre of the neuron layer, the expected number of shared inputs between two layer B neurons is found to be

$$E \left[N^{AB}; [x_i, y_i], [x_j, y_j] \right] = \frac{(N^{AB})^2}{\pi (\sigma^{AB})^2 (d_i^2 + d_j^2)} \exp \left(-\frac{d_{ij}^2}{(\sigma^{AB})^2 (d_i^2 + d_j^2)} \right). \quad (22)$$

We simulated this learning equation and plotted the receptive fields of three layer C neurons in three different positions relative to a small layer of B neurons. The neurons developed radial orientation tuning, with tuning curves showing an orientation directed towards the centre of the lamina.

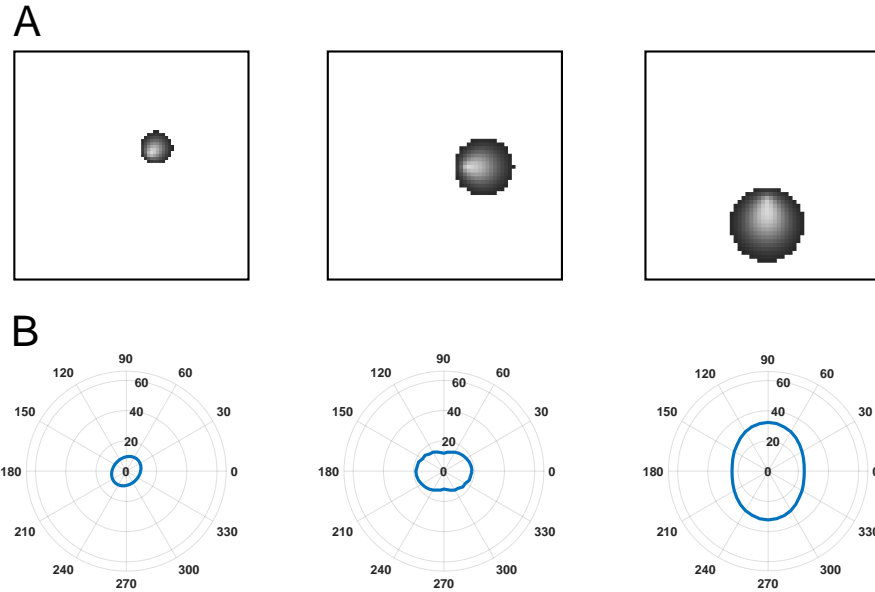


Figure 6: Examples of receptive fields and tuning curves. **(A)** Receptive fields predicted by the leading eigenfunction of three layer *C* neurons at different locations relative to the centre of layer *B*. The layer is small relative to the receptive field size of the layer *C* neurons to highlight changes in receptive field size and the radial orientation selectivity of selected layer *C* neurons. These features emerge from a linearly increasing arbor radius in synaptic connectivity between layer *A* and layer *B* neurons. As established by Linsker (1986a), it is the overlap between the arbors of layer *B* neurons that prompts correlation in their activity despite only inputting unstructured noise into layer *A* and, subsequently, generates the structured receptive fields found in the layer *C* neurons. **(B)** Tuning curves generated for each of the layer *C* neurons in panel *A*. Tuning curves were calculated for the spatial frequency prompting the largest response in the neuron.

5 Discussion

In this paper, we provide a general expression for the complete set of eigenfunctions for the three-layer feed-forward network proposed by Linsker (1986a). Initially, the homeostatic parameters were set to zero to simplify the learning equation. This result was then extended via a perturbation analysis to provide the complete set of eigenfunctions for the network with non-zero homeostatic parameters.

Linsker’s (1986a) analysis was integral in revealing how neural learning occurred before the onset of structured environmental input, empirically demonstrating the emergence of spatial opponent neurons in the third layer. MacKay and Miller (1990) provided a stability analysis of Linsker’s (1986a) network, noting the first six eigenfunctions, determined via an ansatz based on the results of Tang (1990). MacKay and Miller (1990) showed that the receptive field structure of cells in the third layer could be either spatial opponent neuron or bi-lobed neurons, depending upon the value of the homeostatic parameters. Similarly, Walton and Bisset (1992) extended Linsker’s (1986a) network to the auditory system, considering the morphology of the resulting neuron based on the homeostatic parameters of the system. In this paper, we provide the complete set of eigenvalues for the full learning equation, enabling an exact calculation of the homeostatic parameters required to induce this change, and a quantitative analysis on the parameter space.

Linsker (1986b) showed that augmenting the network with additional layers prompts the development of orientation selective neurons. However, given the absence of a complete mathematical framework for the three-layer network, there has been limited mathematical analysis provided for the development of orientation selective neurons in Linsker’s (1986b) network. Yamakazi (2002) provided an analysis of deeper layers, essentially based on an ansatz for the eigenfunctions for the three-layer network. The results in this paper provide the foundation for analysis of larger networks and hence the development

of features other than spatial opponent neurons. As the system is radially symmetric in connectivity distribution, radial eigenfunctions provide a natural coordinate system that will facilitate future work on more complex network and parameter regimes.

The results of this study demonstrate that relaxing the assumption of evenly distributed neurons across the layer can change the receptive fields that emerge in the third layer. Similar to the distribution in the retina, we examined a decrease in neuron density with increasing distance from the centre of the layer and, consequently, an increase in synaptic connectivity radius. We analytically derived an expression for the learning equation in the third layer, as a result of a radially dependent connectivity distribution between the first and second layers. The eigenfunctions for the learning equation were empirically calculated, showing that orientation selective neurons emerge. Interestingly, the preferred orientation of the neurons was the radial orientation towards the centre of the laminar.

It is well established that neural density changes as a function of eccentricity in the retina (Sjöstrand et al., 1999; Watson, 2014), and receptive field sizes of neurons in the primary visual cortex increase with stimulus eccentricity (Wurbs et al., 2013; Smith et al., 2001). Furthermore, it is known that orientation selectivity in the primary visual cortex is biased towards radial orientation, in that an orientation selective neuron in the primary visual cortex is more likely to be oriented towards the centre of the retina (Rodionova et al., 2004). Our results provide a mechanism, based upon the network configuration and neural plasticity, to account for this observed emergence of radially oriented cells.

Acknowledgements

The authors acknowledge support under the Australian Research Council (ARC) Discovery Projects funding scheme (Project DP140102947). Carlo Beenakker is acknowledged for assistance in evaluating the integral in Eq. (44).

Appendix

A Expected number of shared inputs

To examine network dynamics, it is necessary to ascertain the expected number of shared connections between two neurons. The number of shared connections from a presynaptic layer to two neurons in the postsynaptic layer, say i and j , depends on the radial distance between them since the synaptic connection density for each is a Gaussian function of distance (see Fig. 1). We assume for simplicity and without loss of generality that i and j differ only in their x coordinate so that $d_{ij}^B = x_{mi} - x_{mj}$.

Center the Cartesian coordinates describing a neuron's position in the laminar on one of the postsynaptic neurons, say i , so that the other postsynaptic neuron, say j , lies on the x axis. From Eq. (1), neuron, m , in layer A , has a probability of connecting to neuron i in layer B of $p_N(x_{mi}, y_{mi}; \mathbf{0}, \Sigma^A)$ and a probability of connecting to neuron j in layer B of $p_N(x_{mj}, y_{mj}; \mathbf{0}, \Sigma^A) = p_N(x_{mi} - d_{ij}^B, y_{mi}; \mathbf{0}, \Sigma^A)$. The probability of the presynaptic neuron connecting to both postsynaptic neurons i and j is simply the product of the probability of each individual connection being made. The expected number of common connections can be determined by summing this joint probability over the layer or, in the continuous limit, integrating the joint probability over the layer of presynaptic neurons. If N^{AB} denotes the number of synaptic connections from layer A to a layer B neuron and $N^{BB}(d)$ the number of shared connections between two postsynaptic neurons in layer B separated by a distance of d , then in the continuous limit,

$$N^{BB}(d) = (N^{AB})^2 \iint_{xy} p_N(x, y; \mathbf{0}, \Sigma^A) p_N(x - d, y; \mathbf{0}, \Sigma^A) dx dy, \quad (23)$$

where the sub- and super-scripts on distance parameters have been dropped to aid readability. This can be expanded as

$$\begin{aligned}
N^{BB}(d) &= (N^{AB})^2 \iint_{xy} \frac{1}{(\pi(\sigma^{AB})^2)^2} \exp\left(-\frac{x^2+y^2}{(\sigma^{AB})^2}\right) \exp\left(-\frac{(x-d)^2+y^2}{(\sigma^{AB})^2}\right) dx dy \\
&= \frac{(N^{AB})^2}{(\pi(\sigma^{AB})^2)^2} \iint_{xy} \exp\left(-\frac{2x^2+2y^2+d^2-2xd}{(\sigma^{AB})^2}\right) dx dy \\
&= \frac{(N^{AB})^2}{(\pi(\sigma^{AB})^2)^2} \iint_{xy} \exp\left(-\frac{2\left(\left(x-\frac{d}{2}\right)^2+y^2+\frac{d^2}{4}\right)}{(\sigma^{AB})^2}\right) dx dy.
\end{aligned} \tag{24}$$

Introduce $x' = x - d/2$, so that

$$\begin{aligned}
N^{BB}(d) &= \exp\left(-\frac{d^2}{2(\sigma^{AB})^2}\right) \frac{(N^{AB})^2}{(\pi(\sigma^{AB})^2)^2} \iint_{xy} \exp\left(-\frac{2(x'^2+y^2)}{(\sigma^{AB})^2}\right) dx dy \\
&= \exp\left(-\frac{d^2}{2(\sigma^{AB})^2}\right) \frac{(N^{AB})^2}{(\pi(\sigma^{AB})^2)^2} \sqrt{\frac{\pi(\sigma^{AB})^2}{2}} \sqrt{\frac{\pi(\sigma^{AB})^2}{2}} \\
&= \frac{(N^{AB})^2}{2\pi(\sigma^{AB})^2} \exp\left(-\frac{d^2}{2(\sigma^{AB})^2}\right),
\end{aligned} \tag{25}$$

using the identity $\int_{-\infty}^{\infty} \exp(-ax^2) = \sqrt{\pi/a}$.

This result demonstrates that the number of shared connections between two neurons with Gaussian synaptic connection densities is itself a Gaussian function of the radial distance between the neurons with a variance that is half the value of the synaptic connection density radius. This means that a postsynaptic neuron is expected to have the most common connections with itself, for which $d = 0$. Additionally, for small variance or connection radius, a postsynaptic neuron will share many connections with proximate neighbors, with the number of shared connections falling off quickly with distance. Since the expected number of synaptic inputs is constant, a large connection radius implies that the neuron will have shared connections with neurons comparatively distal to it, since nearby neurons will have comparatively fewer shared connections.

B Covariance of neural activity in layer B

Expressions for the covariance of layer B neurons are derived here. Sample covariance between two postsynaptic neuron rates in layer B, say f_i^B and f_j^B , for neurons i and j , respectively, is calculated as

$$\text{cov}(f_i^B, f_j^B) = \mathbb{E}[f_i^B f_j^B] - \mathbb{E}[f_i^B] \mathbb{E}[f_j^B]. \tag{26}$$

For unitary weights from layer A to layer B, Eq. (4a), can be employed to give

$$\begin{aligned}
\text{cov}(f_i^B, f_j^B) &= \mathbb{E}\left[\left(R_a^B + \sum_m f_m^A\right) \left(R_a^B + \sum_n f_n^A\right)\right] - \mathbb{E}\left[R_a^B + \sum_m f_m^A\right] \mathbb{E}\left[R_a^B + \sum_n f_n^A\right] \\
&= (R_a^B)^2 + 2R_a^B \overline{f^B} + \mathbb{E}\left[\sum_m \sum_n f_m^A f_n^A\right] - \left((R_a^B)^2 + 2R_a^B \overline{f^B} + (N^{AB} \overline{f^B})^2\right) \\
&= \left(\mathbb{E}\left[\sum_m \sum_n f_m^A f_n^A\right] - (N^{AB} \overline{f^B})^2\right).
\end{aligned} \tag{27}$$

Layer A neurons are uncorrelated so that the only non-zero contribution to this sum occurs when a layer A neuron has a synaptic connection to each of the layer B neurons under consideration. In this case the input rates are fully correlated, so that the contribution to covariance is proportional to the layer A firing rate.

C Derivation of radial eigenfunctions

C.1 Simplified learning equation

We start by decomposing the weight functions, $w(r, \theta)$, of Eq. (12), into a sum of independent components that are dense in the space using a Fourier series. Therefore, expressing the exponential in its infinite series form, we get

$$\eta \sum_{l=0}^{\infty} \lambda_l (g_l(r) \cos(l\theta) + \tilde{g}_l(r) \sin(l\theta)) = A(\sigma^{AB})^2 \exp\left(-\frac{r^2}{2} \left(\frac{2(\sigma^{AB})^2 + (\sigma^{BC})^2}{(\sigma^{BC})^2}\right)\right) \int_0^{\infty} d\tilde{r} \tilde{r} \exp\left(-\frac{\tilde{r}^2}{2} \left(\frac{(\sigma^{AB})^2 + (\sigma^{BC})^2}{(\sigma^{BC})^2}\right)\right) \int_0^{2\pi} d\tilde{\theta} \sum_{n=0}^{\infty} (r\tilde{r} \cos(\theta - \tilde{\theta}))^n \frac{1}{n!} \sum_{l'=0}^{\infty} (g_{l'}(\tilde{r}) \cos(l'\tilde{\theta}) + \tilde{g}_{l'}(\tilde{r}) \sin(l'\tilde{\theta})). \quad (28)$$

Rearrange the sum and integral terms to give

$$\eta \sum_{l=0}^{\infty} \lambda_l (g_l(r) \cos(l\theta) + \tilde{g}_l(r) \sin(l\theta)) = A(\sigma^{AB})^2 \exp\left(-\frac{r^2}{2} \left(\frac{2(\sigma^{AB})^2 + (\sigma^{BC})^2}{(\sigma^{BC})^2}\right)\right) \int_0^{\infty} d\tilde{r} \tilde{r} \exp\left(-\frac{\tilde{r}^2}{2} \left(\frac{2(\sigma^{AB})^2 + (\sigma^{BC})^2}{(\sigma^{BC})^2}\right)\right) \sum_{l'=0}^{\infty} \sum_{n=0}^{\infty} \frac{1}{n!} (r\tilde{r})^n \int_0^{2\pi} d\tilde{\theta} \cos^n(\theta - \tilde{\theta}) (g_{l'}(\tilde{r}) \cos(l'\tilde{\theta}) + \tilde{g}_{l'}(\tilde{r}) \sin(l'\tilde{\theta})). \quad (29)$$

Now we consider just the inner integral over $\tilde{\theta}$,

$$\int_0^{2\pi} d\tilde{\theta} (\cos^n(\theta - \tilde{\theta})) (g_{l'}(\tilde{r}) \cos(l'\tilde{\theta}) + \tilde{g}_{l'}(\tilde{r}) \sin(l'\tilde{\theta})). \quad (30)$$

A general expression for $(\cos^n(\phi))$ can be found by writing it as

$$\begin{aligned} \cos^n(\phi) &= \frac{1}{2^n} (e^{-i\phi} + e^{i\phi})^n \\ &= \frac{1}{2^n} \sum_{k=0}^n \binom{n}{k} (e^{-i\phi})^k (e^{i\phi})^{n-k} = \frac{1}{2^n} \sum_{k=0}^n \binom{n}{k} (e^{-i\phi})^{n-k} (e^{i\phi})^k \\ &= \frac{1}{2^n} \sum_{k=0}^n \binom{n}{k} (e^{-i\phi(n-2k)}) = \frac{1}{2^n} \sum_{k=0}^n \binom{n}{k} (+e^{i\phi(n-2k)}) \\ &= \frac{1}{2^{n+1}} \sum_{k=0}^n \binom{n}{k} (e^{-i\phi(n-2k)} + e^{i\phi(n-2k)}) \\ &= \frac{1}{2^n} \sum_{k=0}^n \binom{n}{k} \cos(\phi(n-2k)) \\ &= \begin{cases} \frac{1}{2^{n-1}} \sum_{k=0}^{\frac{n-1}{2}} \binom{n}{k} \cos(\phi(n-2k)), & \text{for } n \text{ odd} \\ \frac{1}{2^n} \binom{n}{\frac{n}{2}} + \frac{1}{2^{n-1}} \sum_{k=0}^{\frac{n}{2}-1} \binom{n}{k} \cos(\phi(n-2k)), & \text{for } n \text{ even} \end{cases} \end{aligned} \quad (31)$$

Application of this result to Eq. (30) gives

$$\begin{aligned}
& \int_0^{2\pi} d\tilde{\theta} \cos^n(\theta - \tilde{\theta}) (g_{l'}(\tilde{r}) \cos(l'\tilde{\theta}) + \tilde{g}_{l'}(\tilde{r}) \sin(l'\tilde{\theta})) \\
&= \frac{1}{2^n} \int_0^{2\pi} d\tilde{\theta} \sum_{k=0}^n \binom{n}{k} \cos((\theta - \tilde{\theta})(n - 2k)) (g_{l'}(\tilde{r}) \cos(l'\tilde{\theta}) + \tilde{g}_{l'}(\tilde{r}) \sin(l'\tilde{\theta})) \\
&= \frac{1}{2^n} \sum_{k=0}^n \binom{n}{k} \int_0^{2\pi} d\tilde{\theta} \cos((\theta - \tilde{\theta})(n - 2k)) g_{l'}(\tilde{r}) \cos(l'\tilde{\theta}) \\
&\quad + \frac{1}{2^n} \sum_{k=0}^n \binom{n}{k} \int_0^{2\pi} d\tilde{\theta} \cos((\theta - \tilde{\theta})(n - 2k)) \tilde{g}_{l'}(\tilde{r}) \sin(l'\tilde{\theta}) \\
&= \frac{1}{2^{n+1}} \sum_{k=0}^n \binom{n}{k} \int_0^{2\pi} d\tilde{\theta} g_{l'}(\tilde{r}) (\cos((\theta - \tilde{\theta})(n - 2k) + l'\tilde{\theta}) + \cos(-(\theta - \tilde{\theta})(n - 2k) + l'\tilde{\theta})) \\
&\quad + \frac{1}{2^{n+1}} \sum_{k=0}^n \binom{n}{k} \int_0^{2\pi} d\tilde{\theta} \tilde{g}_{l'}(\tilde{r}) (\sin((\theta - \tilde{\theta})(n - 2k) + l'\tilde{\theta}) - \sin(-(\theta - \tilde{\theta})(n - 2k) + l'\tilde{\theta})) \\
&= \frac{1}{2^{n+1}} \sum_{k=0}^n \binom{n}{k} \int_0^{2\pi} d\tilde{\theta} g_{l'}(\tilde{r}) (\cos(\theta(n - 2k) + \tilde{\theta}(l' - (n - 2k))) + \cos(\theta(n - 2k) + \tilde{\theta}(l' + (n - 2k)))) \\
&\quad + \frac{1}{2^{n+1}} \sum_{k=0}^n \binom{n}{k} \int_0^{2\pi} d\tilde{\theta} \tilde{g}_{l'}(\tilde{r}) (\sin(\theta(n - 2k) + \tilde{\theta}(l' - (n - 2k))) - \sin(\theta(n - 2k) + \tilde{\theta}(l' + (n - 2k)))) \\
&= \begin{cases} \frac{1}{2^n} \sum_{k=0}^{\frac{n-1}{2}} \binom{n}{k} \int_0^{2\pi} d\tilde{\theta} [g_{l'}(\tilde{r}) (\cos(\theta(n - 2k) + \tilde{\theta}(l' - (n - 2k))) + \cos(\theta(n - 2k) + \tilde{\theta}(l' + (n - 2k)))) \\ \quad + \tilde{g}_{l'}(\tilde{r}) (\sin(\theta(n - 2k) + \tilde{\theta}(l' - (n - 2k))) + \sin(\theta(n - 2k) - \tilde{\theta}(l' + (n - 2k))))], & \text{for } n \text{ odd} \\ \frac{1}{2^{n+1}} \binom{n}{\frac{n}{2}} \int_0^{2\pi} d\tilde{\theta} (\cos(l'\tilde{\theta}) + \sin(l'\tilde{\theta})) \\ \quad + \frac{1}{2^n} \sum_{k=0}^{\frac{n}{2}-1} \binom{n}{k} \int_0^{2\pi} d\tilde{\theta} [g_{l'}(\tilde{r}) (\cos(\theta(n - 2k) + \tilde{\theta}(l' - (n - 2k))) + \cos(\theta(n - 2k) + \tilde{\theta}(l' + (n - 2k)))) \\ \quad + \tilde{g}_{l'}(\tilde{r}) (\sin(\theta(n - 2k) + \tilde{\theta}(l' - (n - 2k))) + \sin(\theta(n - 2k) - \tilde{\theta}(l' + (n - 2k))))], & \text{for } n \text{ even} \end{cases} \quad (32)
\end{aligned}$$

All of the integrals within the binomial sum term will evaluate to zero since the functions are periodic in 2π and centred around a mean of zero, except those for which $l' = n - 2k$, because in these cases the $\tilde{\theta}$ terms cancel, and therefore the integration is over a constant. For odd l' , this can only happen for odd n , and for even l' , this can only happen for even n , when $k = \frac{n-l'}{2}$ such that $0 \leq k \leq \frac{n-1}{2}$. Consequently, the sinusoidal term for which the $\tilde{\theta}$ coefficient is $l' + n - 2k$ will always integrate to 0, since $l' + 2k - n \geq 0$ for all k . The additional term for even n will only be non-zero when l' is 0. Thus equation Eq. (32) evaluates to

$$\begin{aligned}
& \int_0^{2\pi} d\tilde{\theta} \cos^n(\theta - \tilde{\theta}) (g_{l'}(\tilde{r}) \cos(l'\tilde{\theta}) + \tilde{g}_{l'}(\tilde{r}) \sin(l'\tilde{\theta})) \\
&= \begin{cases} \frac{2\pi}{2^{n+1}} \binom{n}{\frac{n}{2}} g_{l'}(\tilde{r}), & \text{for } l' = 0 \text{ and } n \text{ even} \\ \frac{2\pi}{2^n} \binom{n-l'}{\frac{n-l'}{2}} g_{l'}(\tilde{r}) \cos(l'\theta) + \frac{2\pi}{2^n} \binom{n-l'}{\frac{n-l'}{2}} \tilde{g}_{l'}(\tilde{r}) \sin(l'\theta), & \text{for } 0 \leq \frac{n-l'}{2} \leq \frac{n-1}{2} \text{ an integer} \\ 0, & \text{otherwise.} \end{cases} \quad (33)
\end{aligned}$$

Note that for $n - l' \geq 0$ we require $n \geq l'$, and thus the infinite sum over l' in Eq. (29) can be truncated.

Incorporating this result into the infinite sums from Eq. (29), separating the odd and even terms for n and l' , and focusing only on the cosine components for the interim, gives,

$$\begin{aligned}
& \sum_{l'=0}^{\infty} \sum_{n=0}^{\infty} \int_0^{2\pi} d\tilde{\theta} \cos^n(\theta - \tilde{\theta}) g_{l'}(\tilde{r}) \cos(l'\tilde{\theta}) \\
&= \sum_{n=0}^{\infty} \sum_{l'=0}^n \left[\frac{2\pi}{2^{2n}} \binom{2n}{n-l'} g_{2l'}(\tilde{r}) \cos(2l'\theta) + \frac{2\pi}{2^{2n+1}} \binom{2n+1}{n-l'} g_{2l'+1}(\tilde{r}) \cos((2l'+1)\theta) \right] \\
&= \sum_{l'=0}^{\infty} \sum_{n=l'}^{\infty} \left[\frac{2\pi}{2^{2n}} \binom{2n}{n-l'} g_{2l'}(\tilde{r}) \cos(2l'\theta) + \frac{2\pi}{2^{2n+1}} \binom{2n+1}{n-l'} g_{2l'+1}(\tilde{r}) \cos((2l'+1)\theta) \right]. \quad (34)
\end{aligned}$$

Let $n' = n - l'$, so that

$$\begin{aligned}
& \sum_{l'=0}^{\infty} \sum_{n=0}^{\infty} \int_0^{2\pi} d\tilde{\theta} \cos^n(\theta - \tilde{\theta}) g_{l'}(\tilde{r}) \cos(l'\tilde{\theta}) \\
&= \sum_{l'=0}^{\infty} \sum_{n'=0}^{\infty} \left[\frac{2\pi}{2^{2(n'+l')}} \binom{2(n'+l')}{n'} g_{2l'}(\tilde{r}) \cos(2l'\theta) + \frac{2\pi}{2^{2(n'+l')+1}} \binom{2(n'+l')+1}{n'} g_{2l'+1}(\tilde{r}) \cos((2l'+1)\theta) \right]. \quad (35)
\end{aligned}$$

Note that n' and l' can now be set independently so that the odd and even terms for l' can now be recombined.

$$\sum_{l'=0}^{\infty} \sum_{n'=0}^{\infty} \int_0^{2\pi} d\tilde{\theta} \cos^n(\theta - \tilde{\theta}) g_{l'}(\tilde{r}) \cos(l'\tilde{\theta}) = \sum_{l'=0}^{\infty} \sum_{n'=0}^{\infty} \frac{2\pi}{2^{2n'+l'}} \binom{2n'+l'}{n'} g_{l'}(\tilde{r}) \cos(l'\theta). \quad (36)$$

Incorporating this sum into the full equation for Eq. (29), gives,

$$\begin{aligned}
& \eta \sum_{l=0}^{\infty} \lambda_l (g_l(r) \cos(l\theta) + \tilde{g}_l(r) \sin(l\theta)) \\
&= A(\sigma^{AB})^2 \exp\left(-\frac{r^2}{2} \left(\frac{2(\sigma^{AB})^2 + (\sigma^{BC})^2}{(\sigma^{BC})^2}\right)\right) \int_0^{\infty} d\tilde{r} \tilde{r} \exp\left(-\frac{\tilde{r}^2}{2} \left(\frac{2(\sigma^{AB})^2 + (\sigma^{BC})^2}{(\sigma^{BC})^2}\right)\right) \\
&\quad \sum_{l'=0}^{\infty} \sum_{n'=0}^{\infty} \binom{2n'+l'}{n'} \frac{1}{(2n'+l')!} (r\tilde{r})^{2n'+l'} \frac{2\pi}{2^{2n'+l'}} (g_{l'}(\tilde{r}) \cos(l'\theta) + \tilde{g}_{l'}(\tilde{r}) \sin(l'\theta)) \\
&= A(\sigma^{AB})^2 \exp\left(-\frac{r^2}{2} \left(\frac{2(\sigma^{AB})^2 + (\sigma^{BC})^2}{(\sigma^{BC})^2}\right)\right) \int_0^{\infty} d\tilde{r} \tilde{r} \exp\left(-\frac{\tilde{r}^2}{2} \left(\frac{2(\sigma^{AB})^2 + (\sigma^{BC})^2}{(\sigma^{BC})^2}\right)\right) \\
&\quad \sum_{l'=0}^{\infty} \sum_{n'=0}^{\infty} \frac{2\pi}{n'!(n'+l')!} \left(\frac{r\tilde{r}}{2}\right)^{2n'+l'} (g_{l'}(\tilde{r}) \cos(l'\theta) + \tilde{g}_{l'}(\tilde{r}) \sin(l'\theta)) \\
&= 2\pi A(\sigma^{AB})^2 \exp\left(-\frac{r^2}{2} \left(\frac{2(\sigma^{AB})^2 + (\sigma^{BC})^2}{(\sigma^{BC})^2}\right)\right) \int_0^{\infty} d\tilde{r} \tilde{r} \exp\left(-\frac{\tilde{r}^2}{2} \left(\frac{2(\sigma^{AB})^2 + (\sigma^{BC})^2}{(\sigma^{BC})^2}\right)\right) \\
&\quad \sum_{l'=0}^{\infty} \sum_{n'=0}^{\infty} \frac{1}{n'!\Gamma(n'+l'+1)} \left(\frac{r\tilde{r}}{2}\right)^{2n'+l'} (g_{l'}(\tilde{r}) \cos(l'\theta) + \tilde{g}_{l'}(\tilde{r}) \sin(l'\theta)) \\
&= 2\pi A(\sigma^{AB})^2 \exp\left(-\frac{r^2}{2} \left(\frac{2(\sigma^{AB})^2 + (\sigma^{BC})^2}{(\sigma^{BC})^2}\right)\right) \\
&\quad \sum_{l'=0}^{\infty} \int_0^{\infty} d\tilde{r} \tilde{r} \exp\left(-\frac{\tilde{r}^2}{2} \left(\frac{2(\sigma^{AB})^2 + (\sigma^{BC})^2}{(\sigma^{BC})^2}\right)\right) I_{l'}(r\tilde{r}) (g_{l'}(\tilde{r}) \cos(l'\theta) + \tilde{g}_{l'}(\tilde{r}) \sin(l'\theta)), \quad (37)
\end{aligned}$$

where $I_{\alpha}(x)$ is a modified Bessel function of the first kind, of order α , such that

$$I_{\alpha}(x) = \sum_{m=0}^{\infty} \frac{1}{m!\Gamma(m+\alpha+1)} \left(\frac{x}{2}\right)^{2m+\alpha}. \quad (38)$$

We can consider each component in the sum separately, such that

$$\begin{aligned}
& \eta \lambda_l (g_l(r) \cos(l\theta) + \tilde{g}_l(r) \sin(l\theta)) \\
&= 2\pi A(\sigma^{AB})^2 \exp\left(-\frac{r^2}{2} \left(\frac{2(\sigma^{AB})^2 + (\sigma^{BC})^2}{(\sigma^{BC})^2}\right)\right) \int_0^{\infty} d\tilde{r} \tilde{r} \exp\left(-\frac{\tilde{r}^2}{2} \left(\frac{2(\sigma^{AB})^2 + (\sigma^{BC})^2}{(\sigma^{BC})^2}\right)\right) I_{l'}(r\tilde{r}) (g_{l'}(\tilde{r}) \cos(l'\theta) + \tilde{g}_{l'}(\tilde{r}) \sin(l'\theta)). \quad (39)
\end{aligned}$$

To derive the eigenfunctions that satisfy Eq. (39), we require weight functions with an exponential of the same form, and polynomials in r that will be of the same order after evaluating the integral. Furthermore, it is well known that Laguerre polynomials are orthogonal over the interval $[0, \infty)$, with respect to the weight function $x^q \exp(-x)$. Consequently, we propose eigenfunctions of the form

$$g_{l,n}(\tilde{r}) \begin{cases} \cos((l' - n)\theta) \\ \sin((l' - n)\theta) \end{cases} = N_{l,n} \tilde{r}^{l-n} \exp\left(-\frac{\tilde{r}^2}{2C}\right) L_n^{l-n}\left(\frac{\tilde{r}^2}{C}\right) \begin{cases} \cos((l' - n)\theta) \\ \sin((l' - n)\theta) \end{cases}, \quad (40)$$

where the additional index, n , denotes the index into eigenvalues of the same order, l , since the solutions are degenerate, and $N_{l,n}$ is a normalisation factor. L_n^{l-n} is an associated Laguerre polynomial. Since $\int_0^\infty x^p e^{-x} L_q^p(x)^2 dx = (p+q)!/q!$, the normalisation factor can be derived as,

$$N_{l,n} = \begin{cases} \sqrt{\frac{2n!}{\pi l! C (\sigma^{AB})^2}}, & l = n \\ \sqrt{\frac{n!}{\pi l! C^{l-n+1} (\sigma^{AB})^2}}, & \text{otherwise,} \end{cases} \quad (41)$$

where the factor of 2 difference occurs for the case $l = n$, because the integral for the angular component is over $\cos(0\theta)$, a constant.

Separating the cos and sin terms in Eq. (39) since they are independent components, and letting

$$\alpha = \frac{(\sigma^{BC})^2}{2(\sigma^{AB})^2 + (\sigma^{BC})^2} \quad (42)$$

the eigenfunctions must satisfy

$$\begin{aligned} r^{l-n} \exp\left(-\frac{r^2}{2C}\right) L_n^{l-n}\left(\frac{r^2}{C}\right) \cos((l-n)\theta) \\ \stackrel{?}{=} 2\pi A (\sigma^{AB})^2 \exp\left(-\frac{r^2}{2\alpha}\right) \int_0^\infty d\tilde{r} \tilde{r} \exp\left(-\frac{\tilde{r}^2}{2\alpha}\right) \exp\left(\frac{-\tilde{r}^2}{2C}\right) \tilde{r}^{l-n} L_n^{l-n}\left(\frac{\tilde{r}^2}{C}\right) I_{l-n}(r\tilde{r}) \cos((l-n)\theta) \\ = 2\pi A (\sigma^{AB})^2 \exp\left(-\frac{r^2}{2\alpha}\right) \int_0^\infty d\tilde{r} \tilde{r} \exp\left(-\frac{\tilde{r}^2}{2}\left(\frac{\alpha+C}{\alpha C}\right)\right) \tilde{r}^{l-n} I_{l-n}(r\tilde{r}) L_n^{l-n}\left(\frac{\tilde{r}^2}{C}\right) \cos((l-n)\theta). \end{aligned} \quad (43)$$

Note the following integral, evaluated using Wolfram Research Inc. (2018):

$$\begin{aligned} J_{n,l} &= \int_0^\infty d\tilde{r} \tilde{r} \exp\left(-\frac{\tilde{r}^2}{2B}\right) \tilde{r}^{l-n} I_{l-n}(r\tilde{r}) L_n^{l-n}\left(\frac{\tilde{r}^2}{C}\right) \\ &= B^{l+1} \left(\frac{C-2B}{BC}\right)^n \exp\left(\frac{Br^2}{2}\right) r^{l-n} L_n^{l-n}\left(\frac{B^2 r^2}{C-2B}\right). \end{aligned} \quad (44)$$

Applying this integral to Eq. (43) gives,

$$\begin{aligned} r^{l-n} \exp\left(-\frac{r^2}{2C}\right) L_n^{l-n}\left(\frac{r^2}{C}\right) \cos((l-n)\theta) \\ \stackrel{?}{=} 2\pi A (\sigma^{AB})^2 \exp\left(-\frac{r^2}{2\alpha}\right) \left(\frac{\alpha C}{\alpha+C}\right)^{l+1} \left(\frac{C-2\left(\frac{\alpha+C}{\alpha C}\right)}{\left(\frac{\alpha+C}{\alpha C}\right)C}\right)^n r^{l-n} \exp\left(\left(\frac{\alpha C}{\alpha+C}\right)\frac{r^2}{2}\right) L_n^{l-n}\left(\frac{\left(\frac{\alpha+C}{\alpha C}\right)^2 r^2}{C-2\left(\frac{\alpha+C}{\alpha C}\right)}\right) \cos((l-n)\theta) \\ = 2\pi A (\sigma^{AB})^2 \left(\frac{C\alpha}{\alpha+C}\right)^{l+1} \left(\frac{C-\alpha}{C+\alpha}\right)^n r^{l-n} \exp\left(-\left(\frac{\alpha+C-2\alpha^2 C}{\alpha(\alpha+C)}\right)\frac{r^2}{2}\right) L_n^{l-n}\left(\frac{C\alpha^2 r^2}{C^2-\alpha^2}\right) \cos((l-n)\theta). \end{aligned} \quad (45)$$

For this equivalence to be true, it is necessary to equate terms. After some simplification, it can be seen that equating both the exponential and Laguerre terms requires that,

$$\begin{aligned} \frac{1}{C} &= \frac{C\alpha^2}{C^2-\alpha^2} \\ \rightarrow 0 &= C(\alpha^2-1) + \alpha^2. \end{aligned} \quad (46)$$

Solving this quadratic in C requires,

$$C = \frac{\alpha}{\sqrt{1 - \alpha^2}}, \quad (47)$$

from which condition we finally get,

$$\begin{aligned} r^{l-n} \exp\left(-\frac{r^2}{2C}\right) L_n^{l-n}\left(\frac{r^2}{C}\right) \cos((l-n)\theta) \\ = 2\pi A (\sigma^{AB})^2 \left(\frac{C\alpha}{\alpha+C}\right)^{l+n+1} r^{l-n} \exp\left(-\frac{r^2}{2C}\right) L_n^{l-n}\left(\frac{r^2}{C}\right) \cos((l-n)\theta). \end{aligned} \quad (48)$$

Substituting the radial connection parameters back in using Eq. (42) finally gives,

$$C = \frac{(\sigma^{BC})^2}{2\sigma^{AB}\sqrt{(\sigma^{AB})^2 + (\sigma^{BC})^2}}. \quad (49)$$

Consequently, the eigenfunctions and eigenvalues for the learning equation can be expressed in polar coordinates as,

$$\lambda_{l,n} = 2\pi A \left(\frac{C(\sigma^{BC})^2}{C((\sigma^{AB})^2 + (\sigma^{BC})^2) + (\sigma^{BC})^2} \right)^{l+n+1} \quad (50a)$$

$$\mathbf{v}_{l,n}(r, \theta) = N_{l,n} r^{l-n} \exp\left(-\frac{r^2}{2C}\right) L_n^{l-n}\left(\frac{r^2}{C}\right) \exp(i(l-n)\theta). \quad (50b)$$

C.2 Full learning equation

If the simplified learning equation in Eq. (11) is denoted by H^0 , from the eigenfunctions derived for the simplified learning equation, we know that,

$$\lambda_{l,n}^0 \mathbf{v}_{l,n}^0(r, \theta) = H^0 \mathbf{v}_{l,n}^0(r, \theta). \quad (51)$$

If we perturb the simplified learning equation by adding a small k_2^{BC} , denote the perturbed system by H , and the eigenfunctions of the perturbed system by $\mathbf{v}_{l,n}(r, \theta)$, where l and n determine the order of the eigenfunction, so that

$$H = A \int_0^\infty d\tilde{r} \tilde{r} \int_0^{2\pi} d\tilde{\theta} \left(\exp\left(-\frac{r^2 + \tilde{r}^2 - 2r\tilde{r}\cos(\theta - \tilde{\theta})}{2(\sigma^{AB})^2}\right) + k_2^{BC} \right) \exp\left(-\frac{\tilde{r}^2 + r^2}{(\sigma^{BC})^2}\right) w(\tilde{r}, \tilde{\theta}), \quad (52)$$

and the eigenvectors for the full system, including the perturbation, satisfy

$$\lambda_{l,n} \mathbf{v}_{l,n}(r, \theta) = H \mathbf{v}_{l,n}(r, \theta). \quad (53)$$

The perturbation on the integral operator, denoted H^1 , is then,

$$H^1 = A \int_0^\infty d\tilde{r} \tilde{r} \int_0^{2\pi} d\tilde{\theta} k_2^{BC} \exp\left(-\frac{\tilde{r}^2 + r^2}{(\sigma^{BC})^2}\right) \mathbf{v}_{l,n}^0(r, \theta), \quad (54)$$

and we require the new eigenfunctions to be similar to the eigenfunctions of the simplified learning equation, plus a small perturbation, so that the first order corrections to the eigenfunctions and eigenvalues can be defined as,

$$\mathbf{v}_{l,n}(r, \theta) = \mathbf{v}_{l,n}^0(r, \theta) + \mathbf{v}_{l,n}^1(r, \theta), \quad \lambda_{l,n} = \lambda_{l,n}^0 + \lambda_{l,n}^1. \quad (55)$$

If $W_{l,n}^{m,p} = \int_{-\infty}^\infty dr r \int_0^{2\pi} d\theta \left(\mathbf{v}_{l,n}^0(r, \theta) \right)^* H^1 \mathbf{v}_{m,p}^0(r, \theta)$, for non-degenerate eigenfunctions, , i.e. $l+n \neq m+p$ the first order corrections can be determined by (Kato, 1995)

$$\mathbf{v}_{l,n}^1(r, \theta) = \sum_{l+n \neq m+p} \frac{W_{l,n}^{m,p}}{\lambda_{l,n}^0 - \lambda_{m,p}^0} \mathbf{v}_{m,p}^0(r, \theta) \quad \text{and} \quad \lambda_{l,n}^1 = W_{l,n}^{l,n}, \quad (56)$$

for non-degenerate eigenfunctions, i.e. $l + n \neq m + p$. For degenerate eigenfunctions, where the denominator of Eq. (56) is equal to zero, the first order correction of degenerate eigenfunctions of order $l + n$, can be found as a weighted sum of the degenerate eigenfunctions, where the weights are determined by the eigenvectors of the $(l + n) \times (l + n)$ matrix of $W_{l,n}^{m,p}$ coefficients. Given that the set of degenerate eigenfunctions of order $l + n$ have angular terms with different frequencies the off-diagonal terms of this matrix are 0. Hence, the eigenfunctions of this matrix are simply the terms, $W_{l,n}^{l,n}$. Additionally, where $l \neq n$, the diagonal terms will be zero because the perturbation integrates to 0 for each radii, which can be seen from the equal number of light and dark regions as you traverse from 0 to 2π at a given radius in Fig. 2. Consequently, the only non-zero perturbation term in a set of degenerate eigenfunctions are those for which $l = n$, which happens once, and only where $l + n$ is even.

For a pair of non-degenerate eigenfunctions where they have different angular frequencies the perturbation will also evaluate to zero. However, note that where the values $l - n$ equals $m - p$, so that the angular terms have the same frequency, some non-zero terms can appear. However, these terms are very small so can be ignored for the purposes of the perturbation approximation. It is therefore only necessary to evaluate the diagonal terms, which are denoted by the single index pair, $W_{l,n}$, and can be evaluated as,

$$\begin{aligned} W_{l,n} &= 2\pi A N_{l,n}^2 \int_0^\infty d\tilde{r} \tilde{r} \tilde{r}^{2(l-n)} \exp\left(-\frac{r^2}{C}\right) \exp\left(-\frac{\tilde{r}^2 + r^2}{(\sigma^{BC})^2}\right) \left[L_n^{l-n}\left(\frac{r^2}{C}\right) \right]^2 \\ &= \pi A N_{l,n}^2 C^{l+n+1} \exp\left(-\frac{r^2}{(\sigma^{BC})^2}\right) \int_0^\infty dz z^{l-n} \exp(-\alpha z) \left[L_n^{l-n}(z) \right]^2, \end{aligned} \quad (57)$$

where $\alpha = \frac{(\sigma^{BC})^2 + C}{(\sigma^{BC})^2}$. This integral on the right hand side can be evaluated as (Gradshteyn and Ryzhik, 2007),

$$\int_0^\infty e^{-bx} x^a L_n^a(x) L_m^a(x) dx = \frac{\Gamma(m+n+a+1)(b-1)^{n+m}}{m!n!b^{m+n+a+1}} {}_2F_1\left(-m, -n; -m-n-a; \frac{b(b-2)}{(b-1)^2}\right), \quad (58)$$

where ${}_2F_1()$ is the hypergeometric function, and hence,

$$W_{l,n} = \pi C^{l-n+1} k_2^{BC} N_{l,n}^2 \frac{\Gamma(l+n+1)(\alpha-1)^{2n}}{n!^2 \alpha^{l+n+1}} {}_2F_1\left(-n, n; l-n; \frac{\alpha(\alpha-2)}{(\alpha-1)^2}\right). \quad (59)$$

Since only the diagonal terms are non-zero, the shape of the perturbed eigenfunctions remains the same as those for the simplified learning equation, given in Eq. (40), but the eigenvalues change according to

$$\lambda_{l,n} = \lambda_{l,n}^0 + W_{l,n}. \quad (60)$$

D Derivation of Cartesian eigenfunctions

To characterise learning in terms of the eigenfunctions it is useful to approximate the system in Eq. (5) by its continuous limit, and initially simplify the system by assuming that $k_2 = 0$. In this case we need to solve the eigenvalue problem that integrates the expected covariance over the layer, weighted by the probability of connection to the postsynaptic neuron, i , in layer C . That is, we need to solve the following eigenfunction equation,

$$\begin{aligned} \lambda \eta w(\mathbf{x}) &= A \int_{-\infty}^\infty \int_{-\infty}^\infty Q(f_j^B, f_i^B) \exp\left(-\frac{|\mathbf{x}'|^2}{(\sigma^{BC})^2}\right) \exp\left(-\frac{|\mathbf{x}|^2}{(\sigma^{BC})^2}\right) w(\mathbf{x}') d^2 \mathbf{x}' \\ &= A \int_{-\infty}^\infty \int_{-\infty}^\infty \exp\left(-\frac{|\mathbf{x} - \mathbf{x}'|^2}{2(\sigma^{AB})^2}\right) \exp\left(-\frac{|\mathbf{x}'|^2}{(\sigma^{BC})^2}\right) \exp\left(-\frac{|\mathbf{x}|^2}{(\sigma^{BC})^2}\right) w(\mathbf{x}') d^2 \mathbf{x}' \\ &= A \exp\left(- (x^2 + y^2) \frac{2(\sigma^{AB})^2 + (\sigma^{BC})^2}{2(\sigma^{AB})^2(\sigma^{BC})^2}\right) \\ &\quad \int_{-\infty}^\infty \int_{-\infty}^\infty \exp\left(-\frac{(2(\sigma^{AB})^2 + (\sigma^{BC})^2)\tilde{x}^2 + 2(\sigma^{BC})^2 x \tilde{x}}{2(\sigma^{AB})^2(\sigma^{BC})^2}\right) \exp\left(-\frac{(2(\sigma^{AB})^2 + (\sigma^{BC})^2)\tilde{y}^2 + 2(\sigma^{BC})^2 y \tilde{y}}{2(\sigma^{AB})^2(\sigma^{BC})^2}\right) w(\mathbf{x}') d\tilde{x} d\tilde{y}, \end{aligned} \quad (61)$$

where $w()$ is the continuous time approximation to w , and neuron m in layer B is denoted by its position vector $\mathbf{x} = (x, y)$, $\mathbf{x}' = (\tilde{x}, \tilde{y})$, and subscripts have been omitted for readability. The coefficient, A , contains the constant terms from the synaptic connection probability (Eq. (1)), such that

$$A = \left(\frac{1}{\pi(\sigma^{AB})^2} \right)^2. \quad (62)$$

Given the separability of the x and y dimensions, in conjunction with the exponential weight function, consider the Hermite polynomial as the form of the eigenfunction, such that the eigenfunctions are given by

$$\mathbf{v}_{u,v} \left(\frac{x}{\sqrt{C}}, \frac{y}{\sqrt{C}} \right) = N_{u,v} \mathbf{H}_u \left(\frac{x}{\sqrt{C}} \right) \mathbf{H}_v \left(\frac{y}{\sqrt{C}} \right) \exp \left(-\frac{x^2 + y^2}{2C} \right), \quad (63)$$

where u and v denote the order of the polynomial for each dimension, giving a two-dimensional eigenfunction of order $u + v$, and $N_{u,v} = \frac{1}{\sqrt{2^u u!}} \frac{1}{\sqrt{2^v v!}}$ is a normalization constant (Roman, 1984). C is a parameter that must be determined.

Consequently, when this expression is input in to the eigenfunction equation from Eq. (61) the learning equation becomes,

$$\begin{aligned} \eta \lambda_{u,v} \mathbf{v}_{u,v} \left(\frac{x}{\sqrt{C}}, \frac{y}{\sqrt{C}} \right) &= A \exp \left(-(x^2 + y^2) \frac{2(\sigma^{AB})^2 + (\sigma^{BC})^2}{2(\sigma^{AB})^2(\sigma^{BC})^2} \right) \int_{-\infty}^{\infty} \int_{-\infty}^{\infty} \exp \left(-\frac{(2(\sigma^{AB})^2 + (\sigma^{BC})^2)\tilde{x}^2 + 2(\sigma^{BC})^2 x \tilde{x}}{2(\sigma^{AB})^2(\sigma^{BC})^2} \right) \\ &\exp \left(-\frac{(2(\sigma^{AB})^2 + (\sigma^{BC})^2)\tilde{y}^2 + 2(\sigma^{BC})^2 y \tilde{y}}{2(\sigma^{AB})^2(\sigma^{BC})^2} \right) \mathbf{v}_{u,v} \left(\frac{\tilde{x}}{\sqrt{C}}, \frac{\tilde{y}}{\sqrt{C}} \right) d\tilde{x} d\tilde{y}, \end{aligned} \quad (64)$$

which holds true only when

$$C = \frac{(\sigma^{BC})^2}{2\sqrt{1 + \frac{(\sigma^{BC})^2}{(\sigma^{AB})^2}}}. \quad (65)$$

Note that this result agrees with the result derived for the radial eigenfunctions, Eq. (13), once the scaling of the r by $1/\sigma^{AB}$ is accounted for.

Due to the separability of the dimensions, the eigenvalues for x and y can be derived independently. Therefore initially consider the problem in just one dimension. In deriving the eigenvalues for the complete orthogonal set of Hermite polynomials, we follow the procedure used in (Wimbauer et al., 1998), and make the Ansatz that,

$$\lambda_u = \Lambda q^u. \quad (66)$$

Using the generating function for one dimensional Hermite polynomials,

$$\exp \left(-t^2 + 2t \frac{x}{\sqrt{C}} \right) = \sum_{l=0}^{\infty} \frac{t^l}{l!} \mathbf{H}_l \left(\frac{x}{\sqrt{C}} \right), \quad (67)$$

and the orthogonality of Hermite polynomials with respect to a Gaussian weight function, we know that,

$$\exp \left(-t^2 + 2t \frac{x}{\sqrt{C}} \right) \exp \left(-\frac{x^2}{2C} \right) = \sum_{l=0}^{\infty} \frac{t^l}{l!} \mathbf{H}_l \left(\frac{x}{\sqrt{C}} \right) \exp \left(-\frac{x^2}{2C} \right). \quad (68)$$

Combining this with Eq. (64), considering a single dimension only, gives,

$$\begin{aligned} \sum_{l=0}^{\infty} \lambda_l \frac{t^l}{l!} \mathbf{H}_l \left(\frac{x}{\sqrt{C}} \right) \exp \left(-\frac{x^2}{2C} \right) &= \sqrt{A} \exp \left(-x^2 \left(\frac{2(\sigma^{AB})^2 + (\sigma^{BC})^2}{2(\sigma^{AB})^2(\sigma^{BC})^2} \right) \right) \\ &\int_{-\infty}^{\infty} \exp \left(-\frac{((2(\sigma^{AB})^2 + (\sigma^{BC})^2)\tilde{x}^2 + 2(\sigma^{BC})^2 x \tilde{x})}{2(\sigma^{AB})^2(\sigma^{BC})^2} \right) \sum_{l=0}^{\infty} \frac{t^l}{l!} \mathbf{H}_l \left(\frac{\tilde{x}}{\sqrt{C}} \right) \exp \left(-\frac{\tilde{x}^2}{2C} \right) d\tilde{x} \\ &= \sqrt{A} \exp \left(-x^2 \left(\frac{2(\sigma^{AB})^2 + (\sigma^{BC})^2}{2(\sigma^{AB})^2(\sigma^{BC})^2} \right) \right) \\ &\int_{-\infty}^{\infty} \exp \left(-\frac{((2(\sigma^{AB})^2 + (\sigma^{BC})^2)\tilde{x}^2 + 2(\sigma^{BC})^2 x \tilde{x})}{2(\sigma^{AB})^2(\sigma^{BC})^2} \right) \exp \left(-t^2 + 2t \frac{\tilde{x}}{\sqrt{C}} \right) \exp \left(-\frac{\tilde{x}^2}{2C} \right) d\tilde{x} \end{aligned} \quad (69)$$

Evaluating the right hand side,

$$\begin{aligned}
\text{RHS} &= \sqrt{A} \exp\left(-x^2 \left(\frac{2(\sigma^{AB})^2 + (\sigma^{BC})^2}{2(\sigma^{AB})^2(\sigma^{BC})^2}\right)\right) \\
&\int_{-\infty}^{\infty} \exp\left(-\frac{((2C(\sigma^{AB})^2 + C(\sigma^{BC})^2 + (\sigma^{AB})^2(\sigma^{BC})^2)\tilde{x}^2 + 2C(\sigma^{BC})^2\tilde{x}x)}{2C(\sigma^{AB})^2(\sigma^{BC})^2}\right) \exp\left(-t^2 + 2t\frac{\tilde{x}}{\sqrt{C}}\right) d\tilde{x} \\
&= \sqrt{A} \exp(-t^2) \exp\left(-x^2 \left(\frac{2(\sigma^{AB})^2 + (\sigma^{BC})^2}{2(\sigma^{AB})^2(\sigma^{BC})^2}\right)\right) \\
&\int_{-\infty}^{\infty} \exp\left(-\frac{(2C(\sigma^{AB})^2 + C(\sigma^{BC})^2 + (\sigma^{AB})^2(\sigma^{BC})^2)\tilde{x}^2 + (2C(\sigma^{BC})^2x + 4t\sqrt{C}(\sigma^{AB})^2(\sigma^{BC})^2)\tilde{x})}{2C(\sigma^{AB})^2(\sigma^{BC})^2}\right) d\tilde{x} \\
&= \sqrt{A} \exp(-t^2) \exp\left(-x^2 \left(\frac{2(\sigma^{AB})^2 + (\sigma^{BC})^2}{2(\sigma^{AB})^2(\sigma^{BC})^2}\right)\right) \exp\left(\frac{(C(\sigma^{BC})^2x + 2t\sqrt{C}(\sigma^{AB})^2(\sigma^{BC})^2)^2}{(2C(\sigma^{AB})^2 + C(\sigma^{BC})^2 + (\sigma^{AB})^2(\sigma^{BC})^2)2C(\sigma^{AB})^2(\sigma^{BC})^2}\right) \\
&\int_{-\infty}^{\infty} \exp\left(-\frac{1}{2C(\sigma^{AB})^2(\sigma^{BC})^2} \left((2C(\sigma^{AB})^2 + C(\sigma^{BC})^2 + (\sigma^{AB})^2(\sigma^{BC})^2)^{\frac{1}{2}}\tilde{x} - \frac{C(\sigma^{BC})^2x + 2t\sqrt{C}(\sigma^{AB})^2(\sigma^{BC})^2}{(2C(\sigma^{AB})^2 + C(\sigma^{BC})^2 + (\sigma^{AB})^2(\sigma^{BC})^2)^{\frac{1}{2}}}\right)^2\right) d\tilde{x} \\
&= \sqrt{A} \exp(-t^2) \left(\frac{2\pi C(\sigma^{AB})^2(\sigma^{BC})^2}{2C(\sigma^{AB})^2 + C(\sigma^{BC})^2 + (\sigma^{AB})^2(\sigma^{BC})^2}\right) \\
&\exp\left(-x^2 \left(\frac{2(\sigma^{AB})^2 + (\sigma^{BC})^2}{2(\sigma^{AB})^2(\sigma^{BC})^2}\right)\right) \exp\left(\frac{(C(\sigma^{BC})^2x + 2t\sqrt{C}(\sigma^{AB})^2(\sigma^{BC})^2)^2}{(2C(\sigma^{AB})^2 + C(\sigma^{BC})^2 + (\sigma^{AB})^2(\sigma^{BC})^2)2C(\sigma^{AB})^2(\sigma^{BC})^2}\right). \tag{70}
\end{aligned}$$

Evaluating the left hand side of Eq. (69) gives

$$\begin{aligned}
\text{LHS} &= \sum_{l=0}^{\infty} \Lambda_0 \frac{(qt)^l}{l!} H_l\left(\frac{x}{\sqrt{C}}\right) \exp\left(-\frac{x^2}{2C}\right) \\
&= \Lambda_0 \exp\left(-qt^2 + \frac{2q}{\sqrt{C}}xt\right) \exp\left(-\frac{x^2}{2C}\right). \tag{71}
\end{aligned}$$

Comparing RHS and LHS requires that

$$q = \frac{C(\sigma^{BC})^2}{2(\sigma^{AB})^2C + (\sigma^{BC})^2C + (\sigma^{AB})^2(\sigma^{BC})^2}, \tag{72}$$

and

$$\begin{aligned}
\Lambda_0 &= \sqrt{\frac{2\pi C(\sigma^{AB})^2(\sigma^{BC})^2}{2C(\sigma^{AB})^2 + 2C(\sigma^{BC})^2 + (\sigma^{AB})^2(\sigma^{BC})^2}} \\
&= \sqrt{2\pi(\sigma^{AB})^2q} \tag{73}
\end{aligned}$$

so that

$$\begin{aligned}
\lambda_l &= \Lambda_0 q^l \\
&= \sqrt{2\pi(\sigma^{AB})^2q} q^{l+\frac{1}{2}}. \tag{74}
\end{aligned}$$

For two dimensions, the final eigenfunctions and eigenvalue pairs, for order u and v , for the x and y dimensions respectively, are given by,

$$\lambda_{u,v} = 2\pi(\sigma^{AB})^2q^{u+v+1} \tag{75a}$$

$$\mathbf{v}_{u,v}\left(\frac{x}{\sqrt{C}}, \frac{y}{\sqrt{C}}\right) = \frac{1}{\sqrt{2^u u!}} \frac{1}{\sqrt{2^v v!}} H_u\left(\frac{x}{\sqrt{C}}\right) H_v\left(\frac{y}{\sqrt{C}}\right) \exp\left(-\frac{x^2 + y^2}{2C}\right). \tag{75b}$$

E Expected number of shared inputs with radially dependent cell density

We consider the expected number of shared inputs between two cells in layer B when there is radially dependent cell density, such that cell density is highest in the centre of the layer, and decreases linearly with distance from the centre. In this case, an assumed consequence is a reduction in the radius of the synaptic connectivity distribution in the layer centre, with a corresponding linear increase with radial distance traversed from the layer centre.

The probability of presynaptic neuron, m , in layer A , generating a synaptic connection to postsynaptic neuron, i , in layer B , is given in Eq. (1).

If neuron j is d_{jc}^B far from the layer centre, with a cell connection density of σ^i , then the expression for the expected number of neurons in layer A connecting to both neuron i and neuron j , in the continuous limit, is given by

$$\begin{aligned} \mathbb{E}[N^{AB}; [x_i, y_j], [x_i, y_j]] &= \frac{(N^{AB})^2}{\pi^2 (\sigma^{AB})^4 d_i^2 d_j^2} \iint \exp\left(-\frac{(x-x_i)^2 + (y-y_i)^2}{d_i^2 (\sigma^{AB})^2}\right) \exp\left(-\frac{(x-x_j)^2 + (y-y_j)^2}{d_j^2 (\sigma^{AB})^2}\right) dx dy, \\ &= \frac{(N^{AB})^2}{\pi^2 (\sigma^{AB})^4 d_i^2 d_j^2} \int_x \exp\left(-\frac{d_j^2 (x-x_i)^2 + d_i^2 (x-x_j)^2}{d_j^2 d_i^2 (\sigma^{AB})^2}\right) dx \int_y \exp\left(-\frac{d_j^2 (y-y_i)^2 + d_i^2 (y-y_j)^2}{d_i^2 d_j^2 (\sigma^{AB})^2}\right) dy, \end{aligned} \quad (76)$$

where we drop the centre subscript, c , and layer superscript, BB , for readability. The exponent in the left sum can be simplified as

$$\begin{aligned} &\frac{d_j^2 (x-x_i)^2 + d_i^2 (x-x_j)^2}{d_i^2 d_j^2 (\sigma^{AB})^2} \\ &= \frac{(d_i^2 + d_j^2) x^2 - 2(d_j^2 x_i + d_i^2 x_j) x + (d_j^2 x_i^2 + d_i^2 x_j^2)}{d_i^2 d_j^2 (\sigma^{AB})^2} \\ &= \frac{d_i^2 + d_j^2}{d_i^2 d_j^2 (\sigma^{AB})^2} \left[x^2 - \frac{2(d_j^2 x_i + d_i^2 x_j)}{d_i^2 + d_j^2} x + \frac{d_j^2 x_i^2 + d_i^2 x_j^2}{d_i^2 + d_j^2} \right] \\ &= \frac{d_i^2 + d_j^2}{d_i^2 d_j^2 (\sigma^{AB})^2} \left[\left(x - \frac{d_j^2 x_i + d_i^2 x_j}{d_i^2 + d_j^2} \right)^2 - \left(\frac{d_j^2 x_i + d_i^2 x_j}{d_i^2 + d_j^2} \right)^2 + \frac{d_j^2 x_i^2 + d_i^2 x_j^2}{d_i^2 + d_j^2} \right] \\ &= \frac{d_i^2 + d_j^2}{d_i^2 d_j^2 (\sigma^{AB})^2} \left[\left(x - \frac{d_j^2 x_i + d_i^2 x_j}{d_i^2 + d_j^2} \right)^2 - \frac{d_j^4 x_i^2 + d_i^4 x_j^2 + 2d_i^2 d_j^2 x_i x_j}{(d_i^2 + d_j^2)^2} + \frac{d_j^2 x_i^2 + d_i^2 x_j^2}{d_i^2 + d_j^2} \right] \\ &= \frac{d_i^2 + d_j^2}{d_i^2 d_j^2 (\sigma^{AB})^2} \left[\left(x - \frac{d_j^2 x_i + d_i^2 x_j}{d_i^2 + d_j^2} \right)^2 - \frac{(d_i^2 + d_j^2)^2 (d_j^2 x_i^2 + d_i^2 x_j^2) + 2d_i^2 d_j^2 x_i x_j - d_i^2 d_j^2 x_i - d_i^2 d_j^2 x_j}{(d_i^2 + d_j^2)^2} + \frac{d_j^2 x_i^2 + d_i^2 x_j^2}{d_i^2 + d_j^2} \right] \\ &= \frac{d_i^2 + d_j^2}{d_i^2 d_j^2 (\sigma^{AB})^2} \left[\left(x - \frac{d_j^2 x_i + d_i^2 x_j}{d_i^2 + d_j^2} \right)^2 - \frac{d_j^2 x_i^2 + d_i^2 x_j^2}{d_i^2 + d_j^2} + \frac{d_j^2 x_i^2 + d_i^2 x_j^2}{d_i^2 + d_j^2} - \frac{d_i^2 d_j^2 (x_i^2 + x_j^2 - 2x_i x_j)}{(d_i^2 + d_j^2)^2} \right] \\ &= \frac{d_i^2 + d_j^2}{d_i^2 d_j^2 (\sigma^{AB})^2} \left(x - \frac{d_j^2 x_i + d_i^2 x_j}{d_i^2 + d_j^2} \right)^2 - \left(\frac{d_i^2 + d_j^2}{d_i^2 d_j^2 (\sigma^{AB})^2} \right) \frac{d_i^2 d_j^2 (x_i^2 + x_j^2 - 2x_i x_j)}{(d_i^2 + d_j^2)^2} \\ &= \frac{d_i^2 + d_j^2}{d_i^2 d_j^2 (\sigma^{AB})^2} \left(x - \frac{d_j^2 x_i + d_i^2 x_j}{d_i^2 + d_j^2} \right)^2 - \frac{(x_i - x_j)^2}{(\sigma^{AB})^2 (d_i^2 + d_j^2)}. \end{aligned}$$

Applying this result to the y integrand in Eq. (76) also, we get

$$\begin{aligned}
E \left[N^{AB}; [x_i, y_i], [x_i, y_i] \right] &= \frac{(N^{AB})^2}{\pi^2 (\sigma^{AB})^4 d_i^2 d_j^2} \int_x \exp \left(-\frac{d_i^2 + d_j^2}{d_i^2 d_j^2 (\sigma^{AB})^2} \left(x - \frac{d_j^2 x_i + d_i^2 x_j}{d_i^2 + d_j^2} \right)^2 - \frac{(x_i - x_j)^2}{(\sigma^{AB})^2 (d_i^2 + d_j^2)} \right) dx \\
&\quad \int_y \exp \left(-\frac{d_i^2 + d_j^2}{d_i^2 d_j^2 (\sigma^{AB})^2} \left(y - \frac{d_j^2 y_i + d_i^2 y_j}{d_i^2 + d_j^2} \right)^2 - \frac{(y_i - y_j)^2}{(\sigma^{AB})^2 (d_i^2 + d_j^2)} \right) dy \\
&= \frac{(N^{AB})^2}{\pi (\sigma^{AB})^4 d_i^2 d_j^2} \exp \left(-\frac{(x_i - x_j)^2 + (y_i - y_j)^2}{(\sigma^{AB})^2 (d_i^2 + d_j^2)} \right) \left(\frac{\pi (\sigma^{AB})^2 d_i^2 d_j^2}{d_i^2 + d_j^2} \right)^{1/2} \left(\frac{\pi (\sigma^{AB})^2 d_i^2 d_j^2}{d_i^2 + d_j^2} \right)^{1/2} \\
&= \frac{(N^{AB})^2}{\pi (\sigma^{AB})^2 (d_i^2 + d_j^2)} \exp \left(-\frac{(x_i - x_j)^2 + (y_i - y_j)^2}{(\sigma^{AB})^2 (d_i^2 + d_j^2)} \right) \\
&= \frac{(N^{AB})^2}{\pi (\sigma^{AB})^2 (d_i^2 + d_j^2)} \exp \left(-\frac{d_{ij}^2}{(\sigma^{AB})^2 (d_i^2 + d_j^2)} \right) \tag{77}
\end{aligned}$$

References

- E. L. Bienenstock, L. N. Cooper, and P. W. Munro. Theory for the development of neuron selectivity: Orientation specificity and binocular interaction in visual cortex. *The Journal of Neuroscience*, 2(1):32–38, 1982.
- W Gerstner, R. Kempter, J. L. van Hemmen, and H. Wagner. A neuronal learning rule for sub-millisecond temporal coding. *Nature*, 383:76–78, 1996.
- G. Goodhill. Contributions of theoretical modeling to the understanding of neural map development. *Neuron*, 56:301–311, 2007.
- I. S. Gradshteyn and I. M. Ryzhik. *Table of integrals, series and products*, chapter 7, page 810. Elsevier, 7th edition, 2007.
- T. Kato. *Perturbation Theory for Linear Operators*, chapter 6, pages 1–643. Springer, second edition, 1995.
- R. Kempter, W. Gerstner, and J. L. van Hemmen. Hebbian learning and spiking neurons. *Physical Review E*, 59(4):4498–4514, 1999a.
- R. Kempter, W. Gerstner, and J. L. van Hemmen. Spike-based compared to rate-based Hebbian learning. *Advances in Neuron Information Processing Systems*, 11:128–131, 1999b.
- R. Linsker. From basic network principles to neural architecture: Emergence of spatial-opponent cells. *Proceedings of the National Academy of Sciences, USA*, 83:7508–7512, 1986a.
- R. Linsker. From basic network principles to neural architecture: Emergence of orientation-selective cells. *Proceedings of the National Academy of Sciences, USA*, 83:8390–8394, 1986b.
- D. J. MacKay and K. D. Miller. Analysis of Linsker’s application of Hebbian rules to linear networks. *Network: Computation in Neural Systems*, 1:257–297, 1990.
- H. Markram, J. Lubke, M. Frotscher, and B. Sakmann. Regulation of synaptic efficacy by coincidence of postsynaptic eps and epsps. *Science*, 275:213–215, 1997.
- K. D. Miller. Correlation-based models of neural development. In M. A. Gluck and D. E. Rumelhart, editors, *Neuroscience and Connectionist Theory*, chapter 7, pages 267–352. Hillsdale, 1990.
- E. I. Rodionova, A. V. Revishchin, and I. N. Pigarev. Distant cortical locations of the upper and lower quadrants of the visual field represented by neurons with elongated and radially oriented receptive fields. *Experimental Brain Research*, 158:373–377, 2004.

- S. Roman, editor. *The Umbral Calculus. Pure and Applied Mathematics*. Academic Press, 1st edition, 1984.
- W. Senn and N. J. Buchs. Spike-based synaptic plasticity and the emergence of direction selective simple cells: Mathematical analysis. *Journal of Computational Neuroscience*, 14:119–138, 2003.
- J. Sjöstrand, V. Olsson, Z. Popovic, and N. Conradi. Quantitative estimations of foveal and extra-foveal circuitry in humans. *Vision Research*, 39(18):2987–2998, 1999.
- A. T. Smith, K. D. Singh, A. L. Williams, and M. W. Greenlee. Estimating receptive field size from fMRI data in human striate and extrastriate visual cortex. *Cerebral Cortex*, 11:1182–1190, 2001.
- D. S. Tang. *Self-organization, emerging properties, and learning*, chapter Information theory and early Visual information processing, pages 113–125. Plenum Press, New York, 1st edition, 1990.
- L. Walton and D. L. Bissest. Parameterising feature sensitive cell formation in Linsker’s networks in the auditory system. In *Neural Information Processing Systems*, pages 1007–1013, 1992.
- A. B. Watson. A formula for human retinal ganglion cell receptive field density as a function of visual field location. *Journal of Vision*, 14(7):15, 2014.
- S. Wimbauer, O. G. Wensch, K. D. Miller, and J. L. van Hemmen. Development of spatiotemporal receptive fields of simple cells: I. Model formulation. *Biological Cybernetics*, 77:453–461, 1997a.
- S. Wimbauer, O. G. Wensch, K. D. Miller, and J. L. van Hemmen. Development of spatiotemporal receptive fields of simple cells: II. Simulation and analysis. *Biological Cybernetics*, 77:463–477, 1997b.
- S. Wimbauer, W. Gerstner, and J. L. van Hemmen. Analysis of a correlation-based model for the development of orientation-selective receptive fields in the visual cortex. *Network: Computation in Neural Systems*, 9:449–466, 1998.
- Wolfram Research Inc. Mathematica, Version 11.3, 2018. Champaign, IL, 2018.
- J. Wurbs, E. Mingolla, and A. Yazdanbakhsh. Modeling a space-variant cortical representation for apparent motion. *Journal of Vision*, 13(10):1–17, 2013.
- T. Yamakazi. A mathematical analysis of the development of oriented receptive fields in Linsker’s model. *Neural Networks*, 15:201–207, 2002.